Global nuclear ground state properties studied by spherical localized RHFB theory

Yanan Huang
Supervisor：Prof. Yifei Niu
Collaborator：Dr. Qiang Zhao, Prof. Pengwei Zhao

Outline

- **Introduction**
- **Theoretical Framework**
- **Numerical Details**
- **Results and Discussions**
  - Mass
  - Charge Radii
  - Shell Gap
  - Spurious Shell Removal
  - α-Decay
  - SHN
- **Summary**

Introduction

- 7000-10000 nuclei are predicted to be bound, while over 2500 nuclei are already measured.

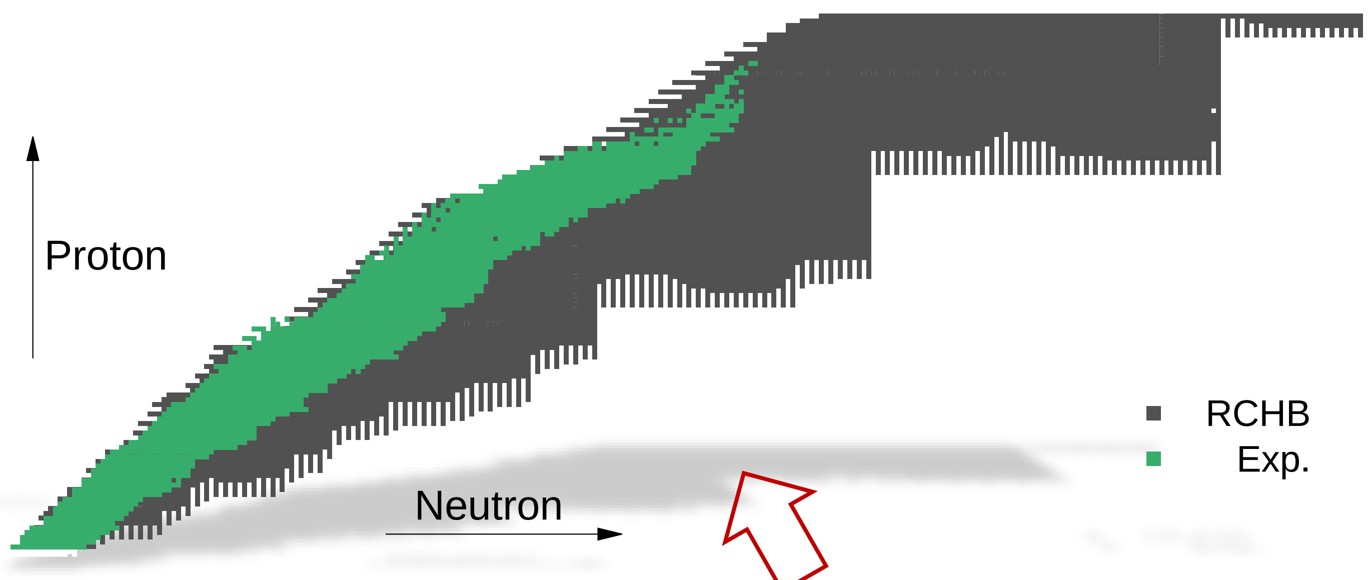

basic input of nucleosynthesis

- Covariant density functional theory (CDFT): powerful for a global description of nuclei.

J. Meng et al.,2016, Relativistic Density Functional for Nuclear Structure

Introduction

- **Global nuclear ground state properties have been studied with CDFT for decades.**

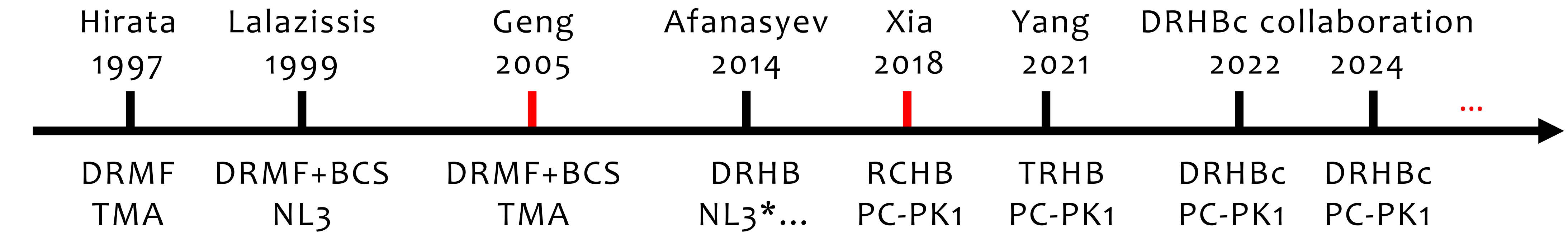

- **The inclusion of exchange terms is important for the description of nuclear properties:**

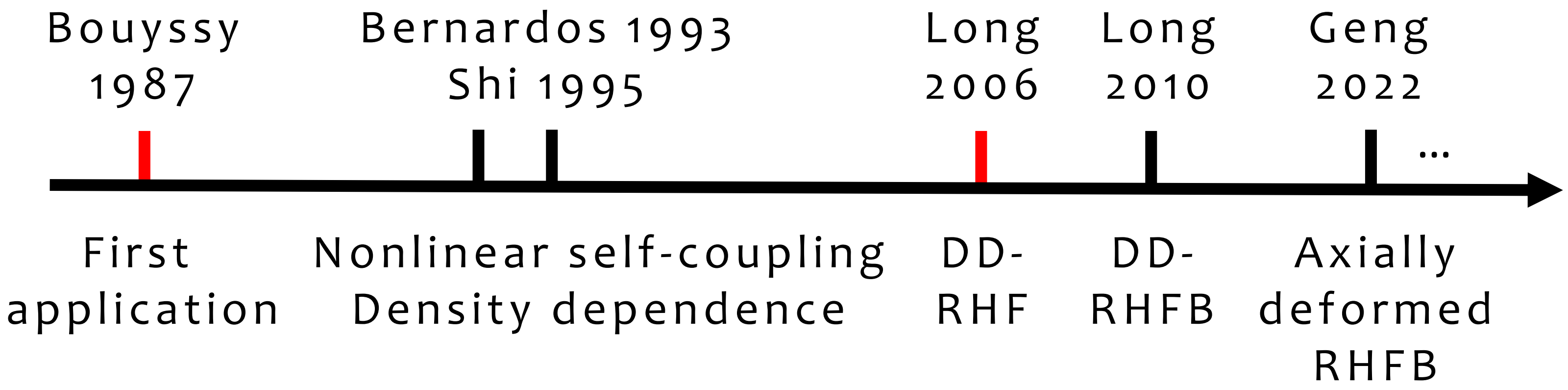

from Prof. W. H. Long's lecture

- ✓ Shell evolution

  W. H. Long et al.,2008,EPL 82,12001

- ✓ Pseudospin(PSO) symmetry restoration

  J. Geng et al.,2019,PRC 100,051301R

- ✓ New magicity

  J. Liu et al.,2019,PLB,806,135524

time consuming! ⇒ hard to be applied in large-scale calculations

- Spurious shell exists in many relativistic density functionals, but it can be cured by **PKA1 with exchange terms**.

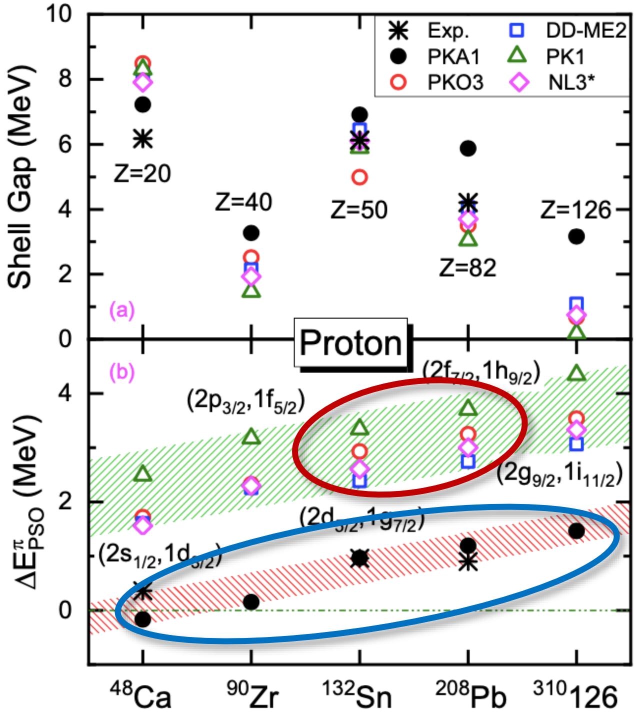

J. Geng et al.,2019,PRC 100,051301R

- PCF-PK1: the point-coupling functional with tensor coupling and with localized exchange terms by Fierz transformation.

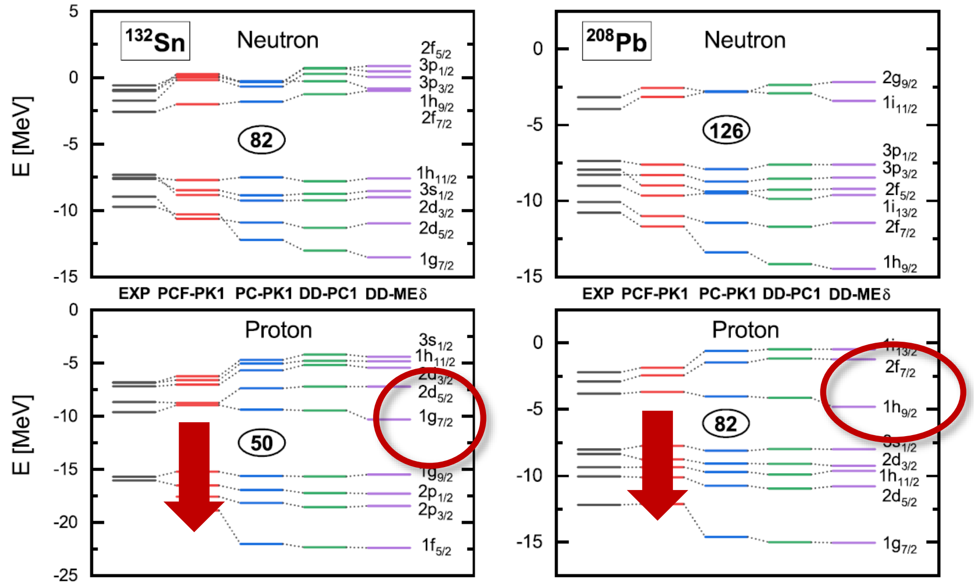

Q. Zhao et al.,2022,PRC 106,034315

- Spurious shells are successfully **eliminated using PCF-PK1** without numerical complexity raised by exchange terms.

In this work, the global nuclear ground state properties with localized exchanged terms will be studied.

Theoretical Framework

- The effective Lagrangian density consists of four parts

$$\mathcal{L} = \bar{\psi}(i\gamma_\mu\partial^\mu - M)\psi - \frac{1}{2}[\alpha_S(\bar{\psi}\psi)(\bar{\psi}\psi) + \alpha_{tS}(\bar{\psi}\vec{\tau}\psi)(\bar{\psi}\vec{\tau}\psi) + \alpha_V(\bar{\psi}\gamma_\mu\psi)(\bar{\psi}\gamma^\mu\psi)$$
$$+\alpha_{tV}(\bar{\psi}\gamma_\mu\vec{\tau}\psi)(\bar{\psi}\gamma^\mu\vec{\tau}\psi) + \alpha_T(\bar{\psi}\sigma_{\mu\nu}\psi)(\bar{\psi}\sigma^{\mu\nu}\psi) + \alpha_{tT}(\bar{\psi}\sigma_{\mu\nu}\vec{\tau}\psi)(\bar{\psi}\sigma^{\mu\nu}\vec{\tau}\psi)$$
$$+\alpha_{PS}(\bar{\psi}\gamma_5\psi)(\bar{\psi}\gamma_5\psi) + \alpha_{tPS}(\bar{\psi}\gamma_5\vec{\tau}\psi)(\bar{\psi}\gamma_5\vec{\tau}\psi) + \alpha_{PV}(\bar{\psi}\gamma_5\gamma_\mu\psi)(\bar{\psi}\gamma_5\gamma^\mu\psi)$$
$$+\alpha_{tPV}(\bar{\psi}\gamma_5\gamma_\mu\vec{\tau}\psi)(\bar{\psi}\gamma_5\gamma^\mu\vec{\tau}\psi)] - \frac{1}{2}\delta_S\partial_\mu(\bar{\psi}\psi)\partial^\mu(\bar{\psi}\psi)$$
$$-e\frac{1-\tau_3}{2}\bar{\psi}\gamma_\mu\psi A^\mu - \frac{1}{4}F_{\mu\nu}F^{\mu\nu}$$

known: $\alpha_S, \alpha_{tS}, \alpha_V, \alpha_{tV}, \alpha_T$

Fierz Transformation ⇒

unknown: $\alpha_{tT}, \alpha_{PS}, \alpha_{tPS}, \alpha_{PV}, \alpha_{tPV}$

exchange terms are treated like direct ones

- The RHB equation is solved in the space of **Harmonic Oscillator(H. O.) basis** and **spherical** approximation.

$$\begin{pmatrix} \hat{h}_D - \lambda & \hat{\Delta} \\ -\hat{\Delta} & -\hat{h}_D^* + \lambda \end{pmatrix} \begin{pmatrix} U_k \\ V_k \end{pmatrix} = E_k \begin{pmatrix} U_k \\ V_k \end{pmatrix}$$

Q. Zhao et al.,2022,PRC 106,034315

Choice of Oscillator Frequency

- Take ^{208}Pb as an example, and reference value: $N_f = 40$.

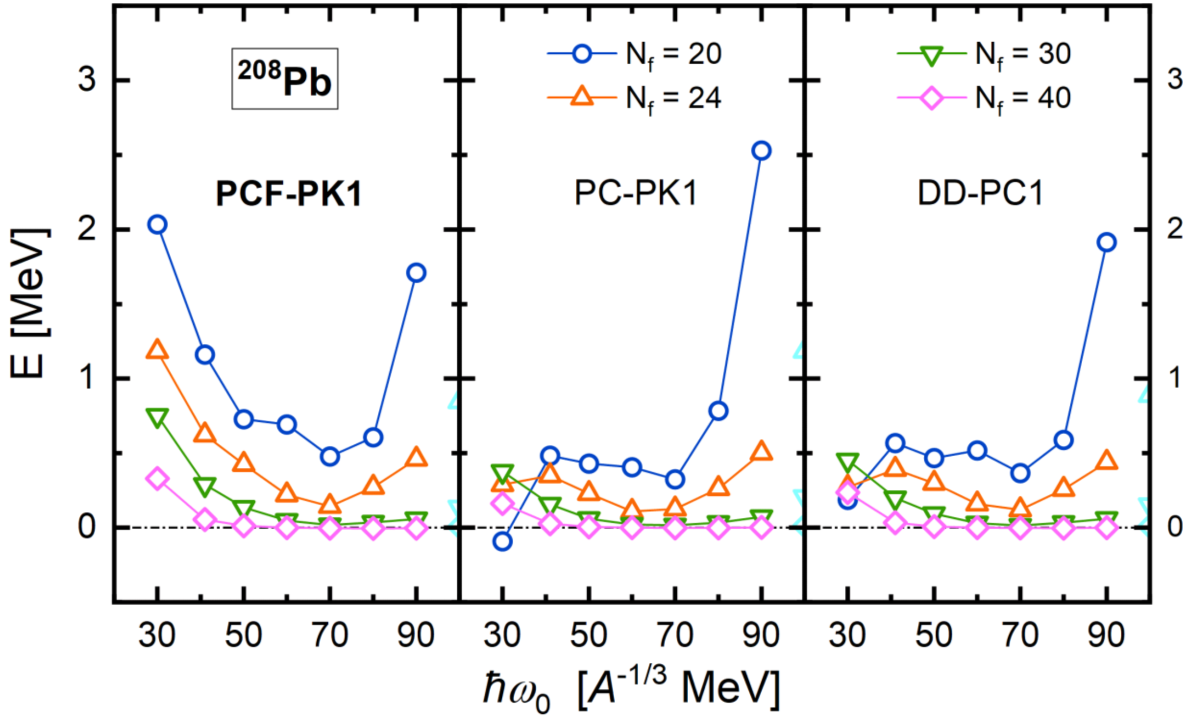

- ✓ Spherical RHB solved by H.O. basis
- ✓ Functional: PCF-PK1
- ✓ Separable pairing: $G = 657.5419$ MeV, $a = 0.644$ fm.

Q. Zhao et al.,2022,PRC 106,034315

For PCF-PK1 the convergence behavior is the best when the H.O. frequency is taken as 70 $A^{-1/3}$ MeV.

Convergence Check

➢ 9 stable nuclei in 3 different regions. Red: the variation of binding energy is within 0.01%.

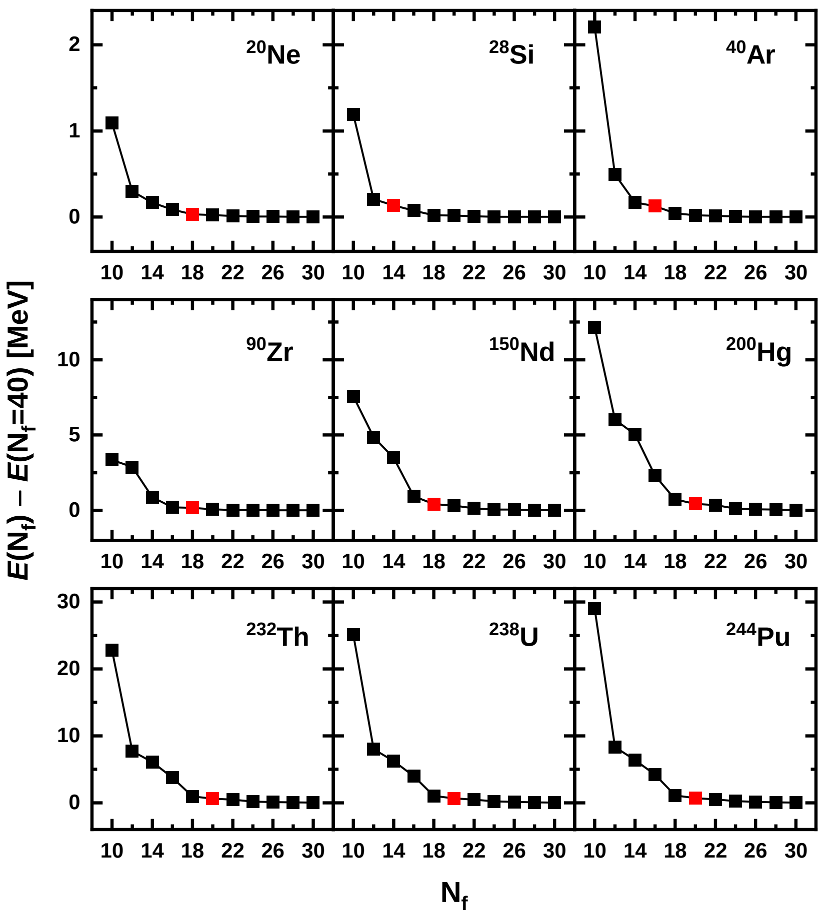

20 harmonic oscillator(H.O.) major shells are used for all the nuclei.

Outline

Mass

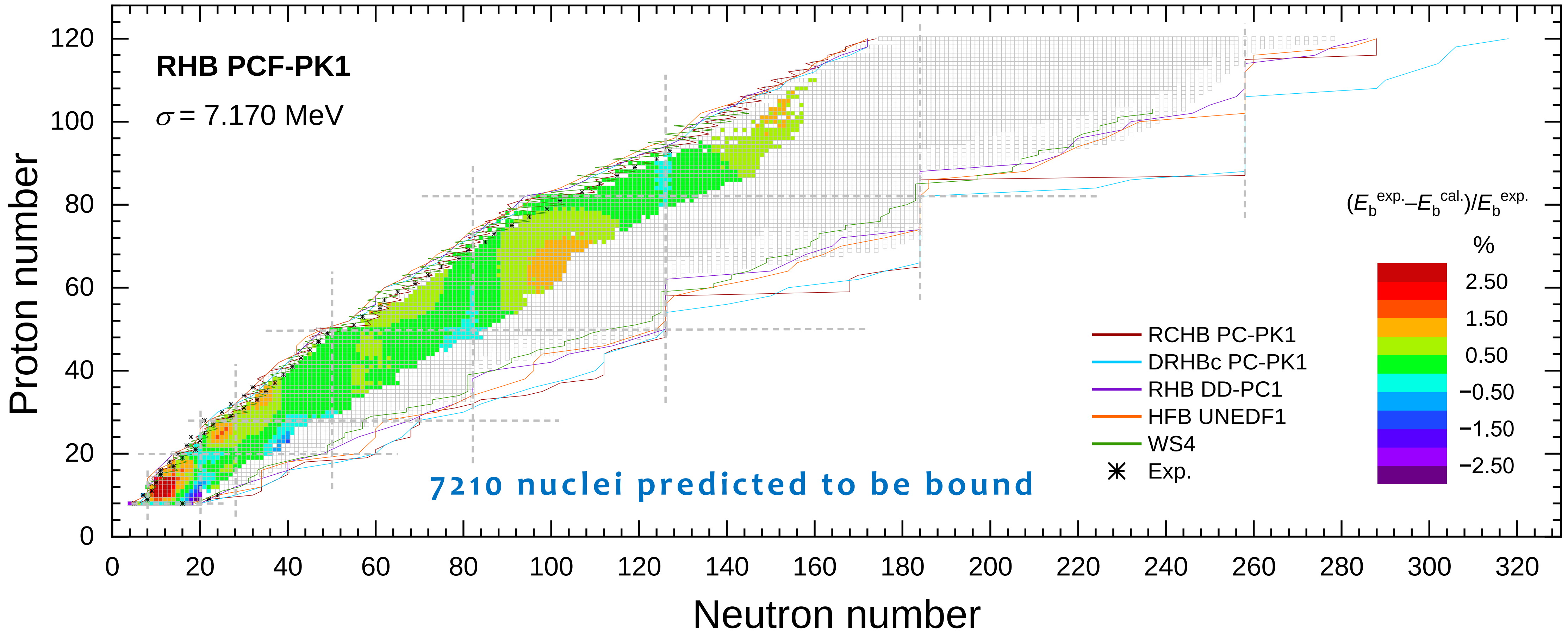

- Overestimation: neutron-rich side in $Z = 8, 20$ and $N = 82, 126$. Underestimation: neutron-deficient side in light region and neutron-rich side near $N = 100$.
- Dripline: close to DD-PC1, UNEDF1, and WS4, but different from PC-PK1 with continuum effect.

Mass

➢ Comparison of mass accuracy with respect to different versions of experimental data.

Exp. data	RHB PCF-PK1	σ_{rms}/MeV	RCHB PC-PK1	σ_{rms}/MeV	
AME2003	2085	6.938	2111	7.884	G.Audi,2003,NPA 729,337
AME2012	**2258**	**7.026**	**2285**	**7.958**	M.Wang,2012,CPC 36,1603
AME2016	2301	6.996	2331	7.917	M.Wang,2017,CPC 41,030003
AME2020	**2351**	**7.170**	**2382**	**8.103**	M.Wang,2021,CPC 45,030003

➢ For magic nuclei: σ (PCF-PK1)=2.034 MeV, σ (RCHB)= 2.157 MeV.

X. W. Xia et al.,2018,ADNDT 121,1

Charge Radii

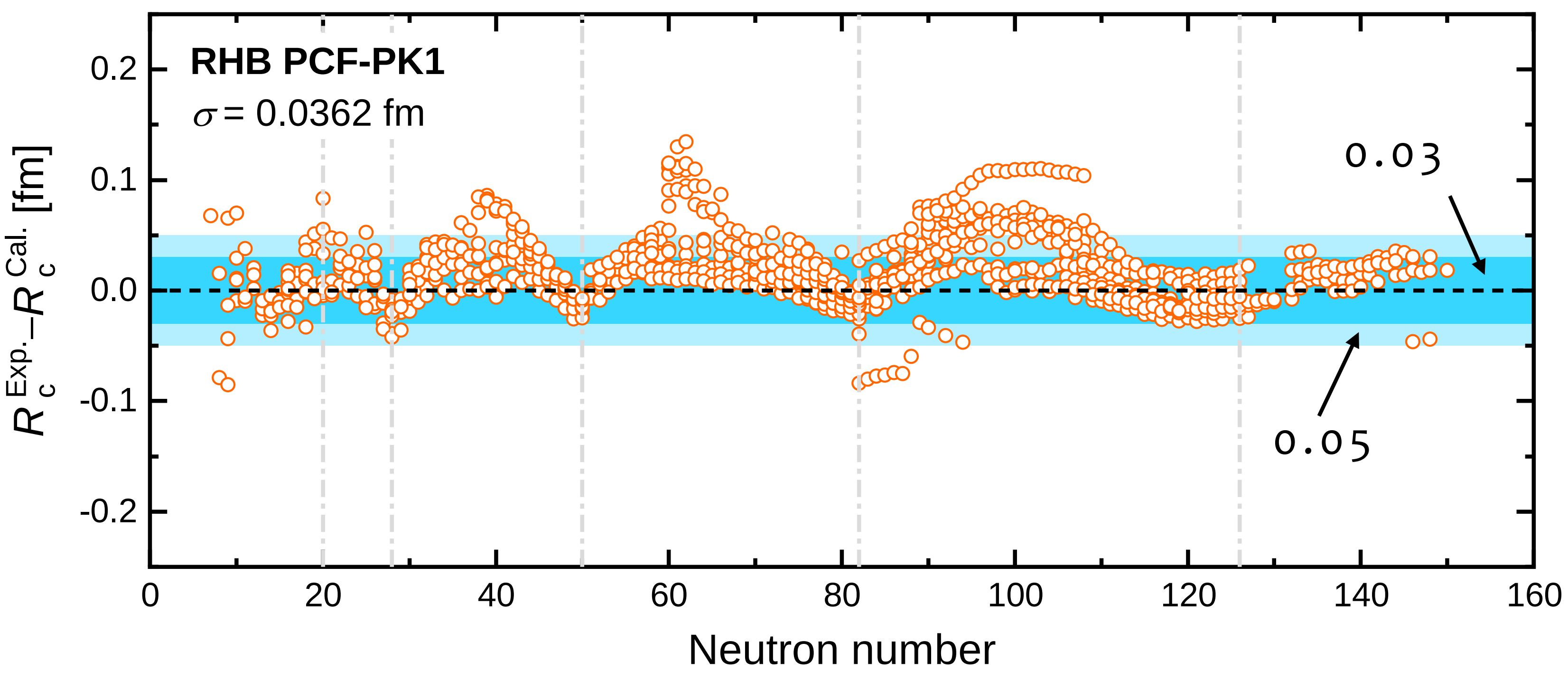

R$_c$(DRHBc) − R$_c$(RCHB)

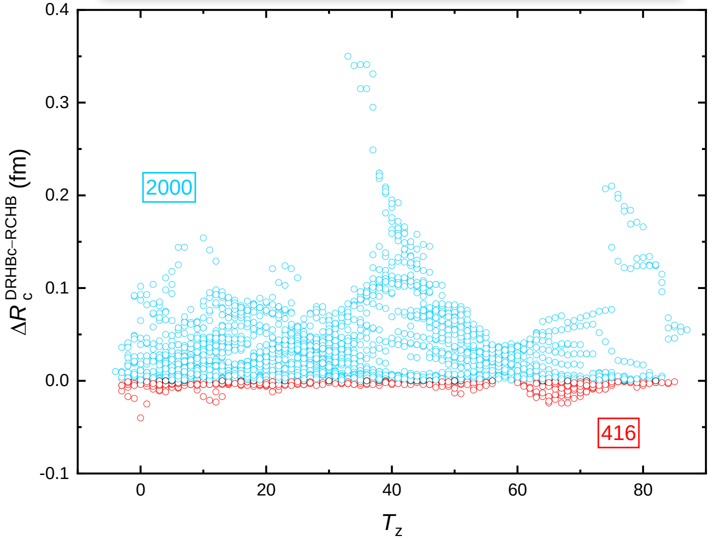

σ(RCHB)=0.0344 fm
σ(DRHBc)=0.0322 fm

K. Zhang et al.,2022,ADNDT 144,101488

1. σ(PCF-PK1)=0.0362 fm, σ(RCHB)=0.0344 fm.
2. 85%: exp±0.05 fm(light blue), 70%: exp±0.03 fm(dark blue).
3. Open-shell nuclei: R_c are underestimated. R_c are expected to increase when deformation effects are considered.

Neutron Shell Gap

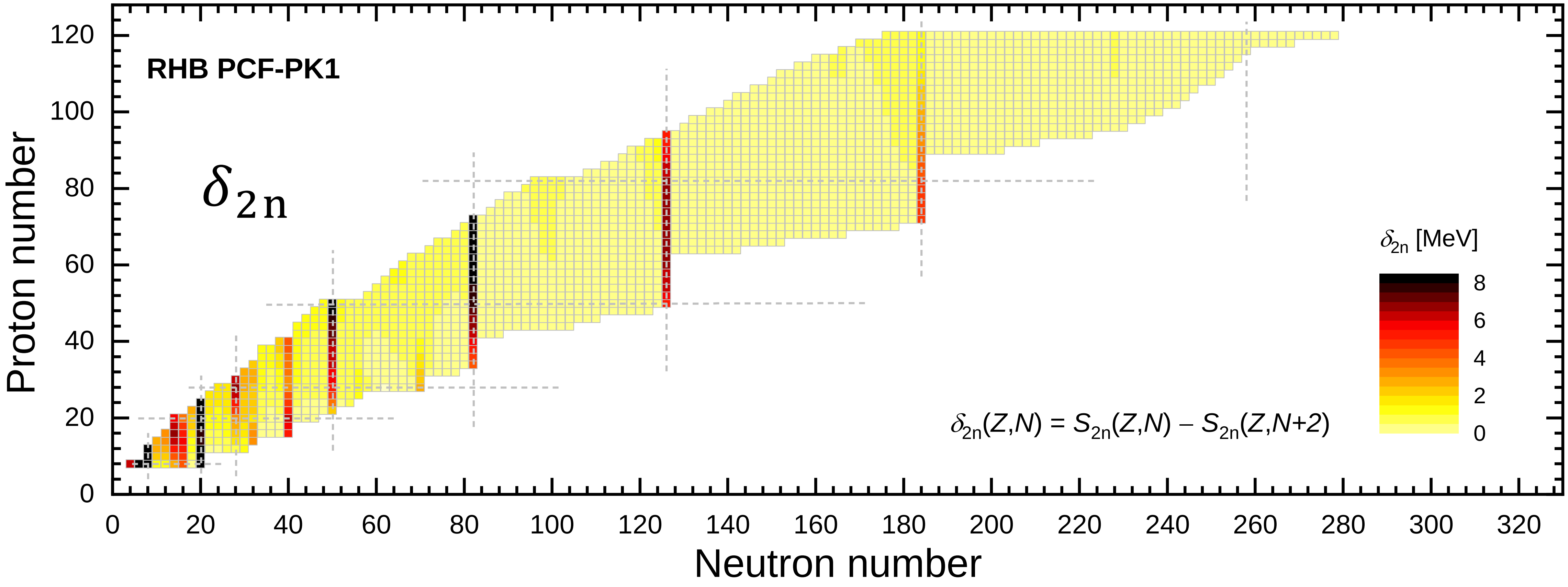

1. Traditional magic number: $N = 8, 20, 28, 50, 82, 126$, and 184.
2. Subshell: $N = 14, 16$.
3. Shell gaps are decreased near the neutron dripline at $N = 28, 50, 82, 126$ and in the superheavy nuclear(SHN) region with $N = 184$.

Proton Shell Gap

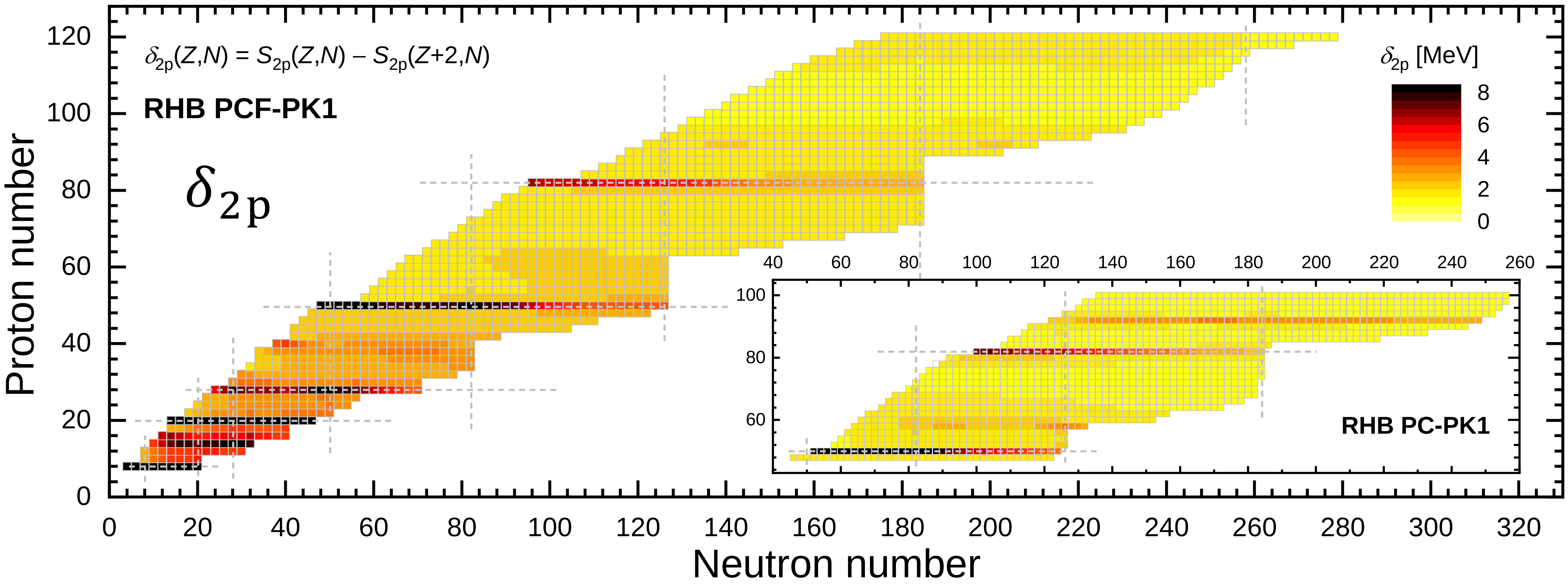

1. Traditional magic number: $Z = 8, 20, 28, 50, 82$. Subshell: $Z = 14, 16$.
2. Spurious shell: $Z = 58, 92$ is removed.
3. Shell gaps are decreased near neutron dripline at $Z = 28, 50, 82$. But not at $Z = 20$, which is the same as PC-PK1.

Overview of Shell Gap

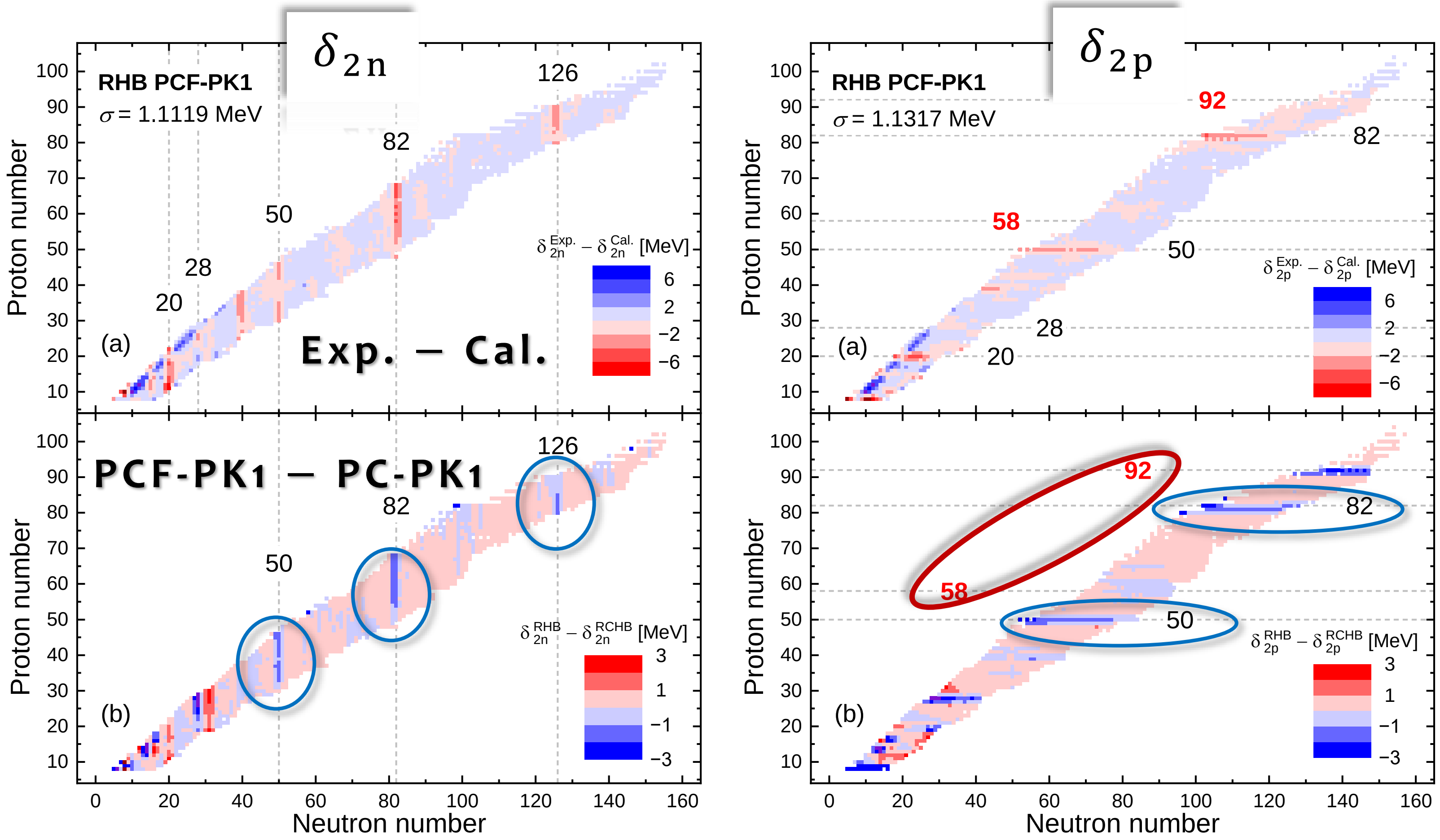

σ /MeV	δ_{2n}	δ_{2p}
PCF-PK1	**1.1119**	**1.1317**
PC-PK1	1.2260	1.3047

1. For magic nuclei: PCF-PK1 and PC-PK1 both overestimate shell gap. But PCF-PK1 improved overestimation, compared with PC-PK1, which means a more reasonable shell structure.
2. For spurious shell $Z = 58, 92$: smaller than PC-PK1.

Spurious Shell Removal

➢ Shell gaps of $Z = 58, 92$ isotopic chain

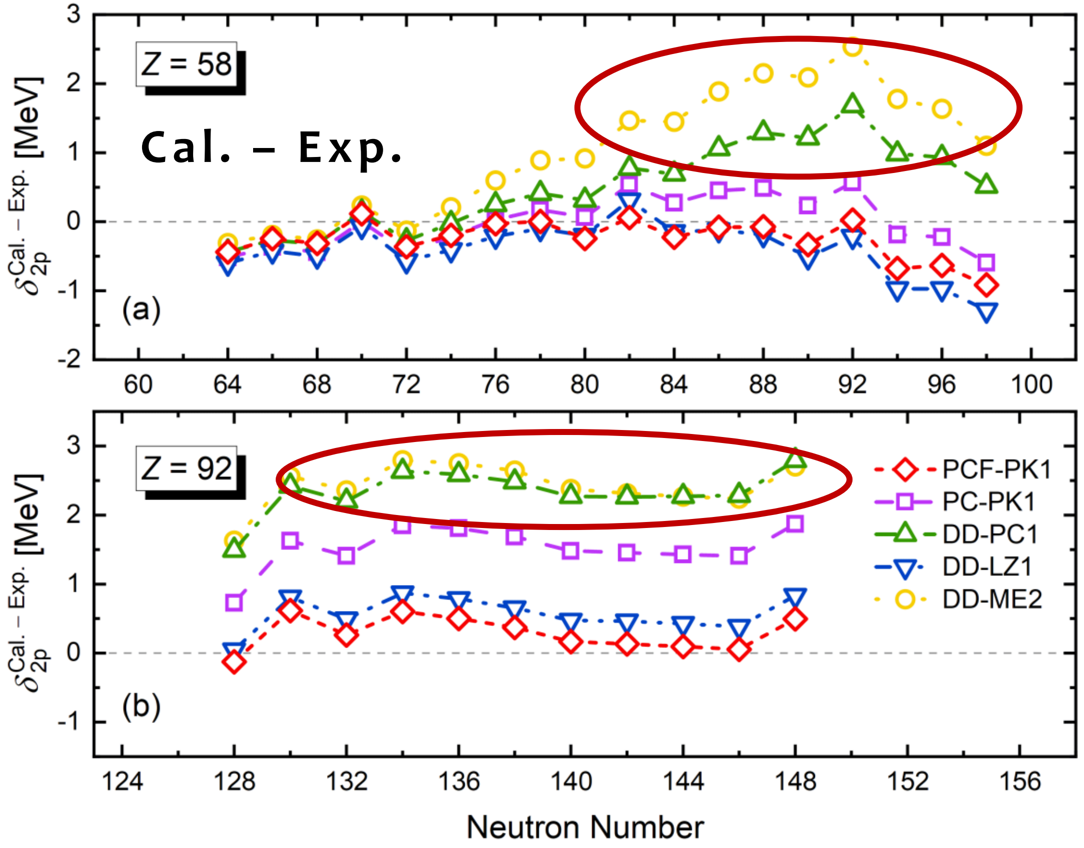

1. Compared with other functionals, PCF-PK1 is closer to the experimental data.
2. PCF-PK1: tensor coupling is included and the constraint $f_S''(1) = f_V''(1)$ is released.

W. H. Long et al.,2007,PRC 76,034314; J. Geng et al.,2019,PRC 100,051301R

Impacts of Spurious Shell Removal

➢ Effects of single particle(s. p.) proton shell gaps on the mass for nuclei ^{140}Ce and ^{218}U.

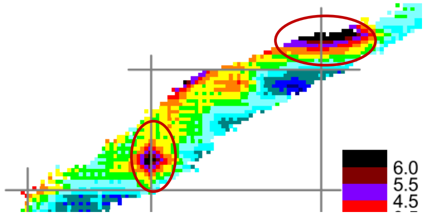

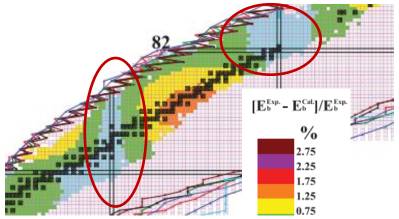

1. Mass overestimation is a problem near ^{140}Ce and ^{218}U.
   L. S. Geng et al.,2005,PTP 113,4,785; X. W. Xia et al.,2018,ADNDT 121,1
2. For doubly magic nuclei: PCF-PK1 is closer to the experiment.
   V. Isakov et al.,2002,EPJA 14,29
3. Compared with other functionals, s. p. proton shell gaps obtained by PCF-PK1 are **smaller**, which improves the mass overestimation.

E_B [MeV]	^{140}Ce	^{218}U
PCF-PK1	1173.5	1667.5
DD-LZ1	1172.0	1666.6
PC-PK1	1174.4	1670.2
DD-PC1	1178.4	1673.5
DD-ME2	1175.4	1673.0
Exp.	1172.7	1665.6

s.p. Proton shell gaps at Z= [MeV]	^{132}Sn		^{140}Ce		^{208}Pb		^{218}U	
	50	58	50	58	82	92	82	92
PCF-PK1	6.25	0.22	5.38	0.87	4.06	1.23	3.93	1.73
DD-LZ1	7.29	1.35	6.71	2.12	5.20	1.55	5.01	2.23
PC-PK1	6.23	2.04	5.85	2.57	4.09	2.57	4.08	3.00
DD-PC1	6.21	2.27	5.83	2.65	3.85	2.96	4.01	3.27
DD-ME2	6.45	2.39	6.02	3.06	4.06	2.75	4.08	3.29
Exp.	6.08	0.96			4.21	0.90		

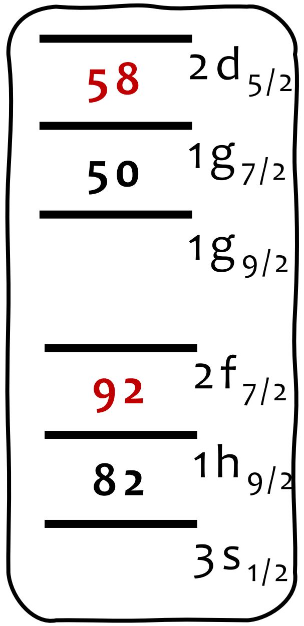

α-Decay Energy

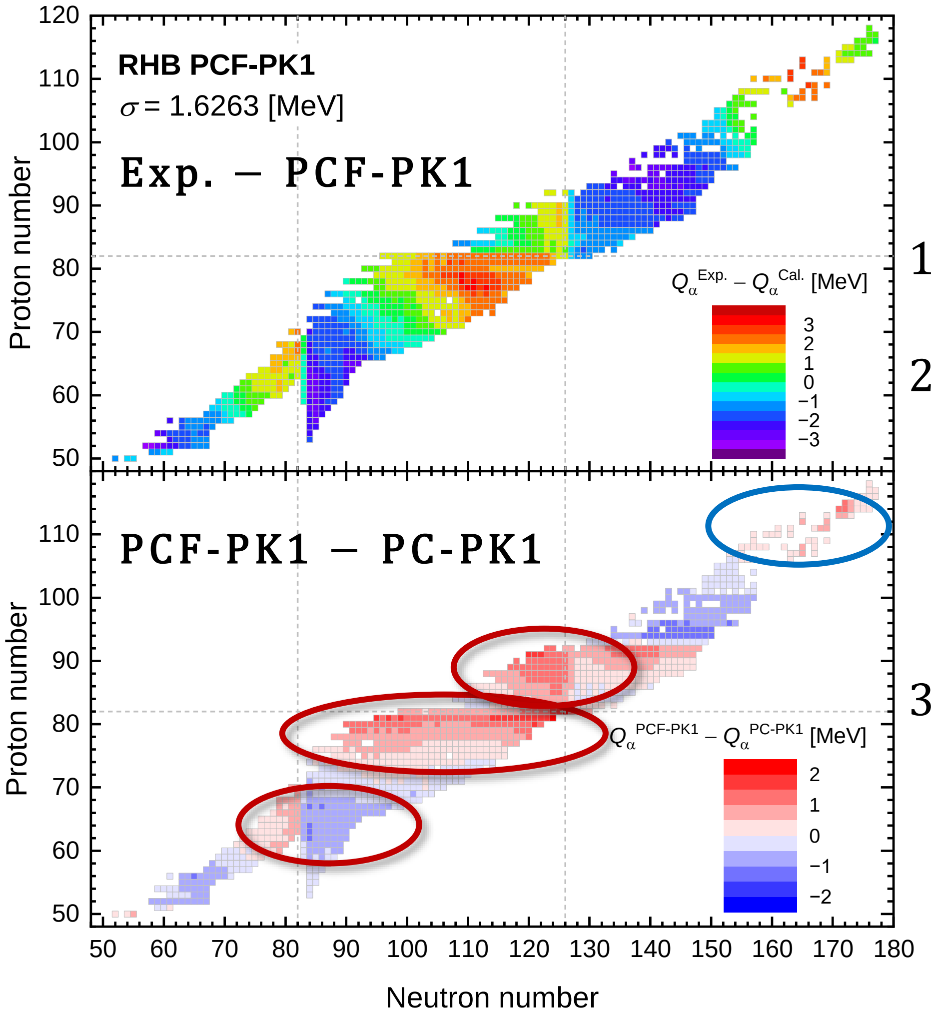

1. σ(PCF-PK1)=1.6263 MeV, σ(RCHB)=2.0801 MeV.
2. Near magic nuclei: obvious difference between PCF-PK1 and PC-PK1. Q_α obtained by PCF-PK1 is closer to the experiment, which implies PCF-PK1 has a more reasonable description of the shell structure.
3. Deformed Superheavy nuclear region($Z > 92$): closer to the experiment.

Shell Gaps in SHN Region

➢ Shell gaps in the region with $Z > 100$. $N_f = 20$ is taken.

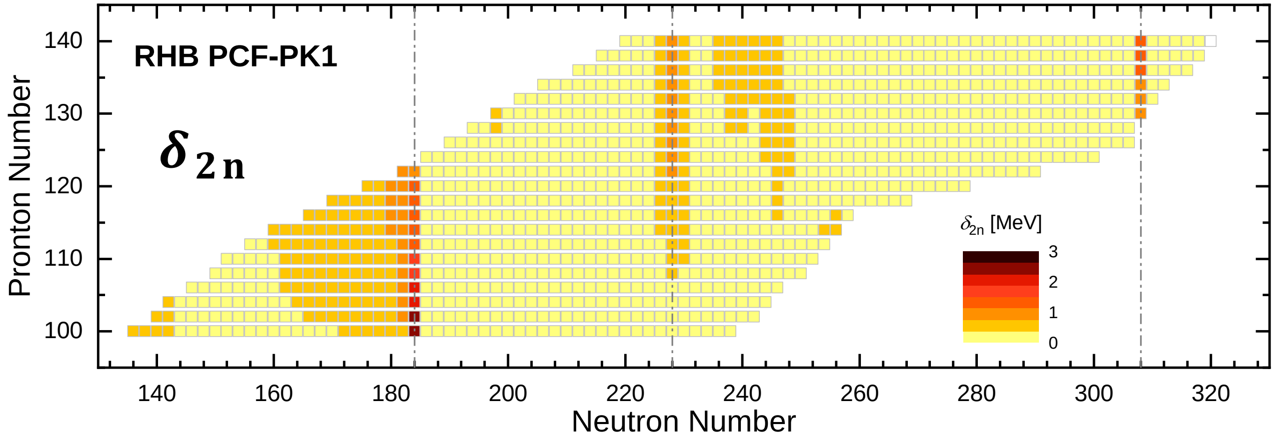

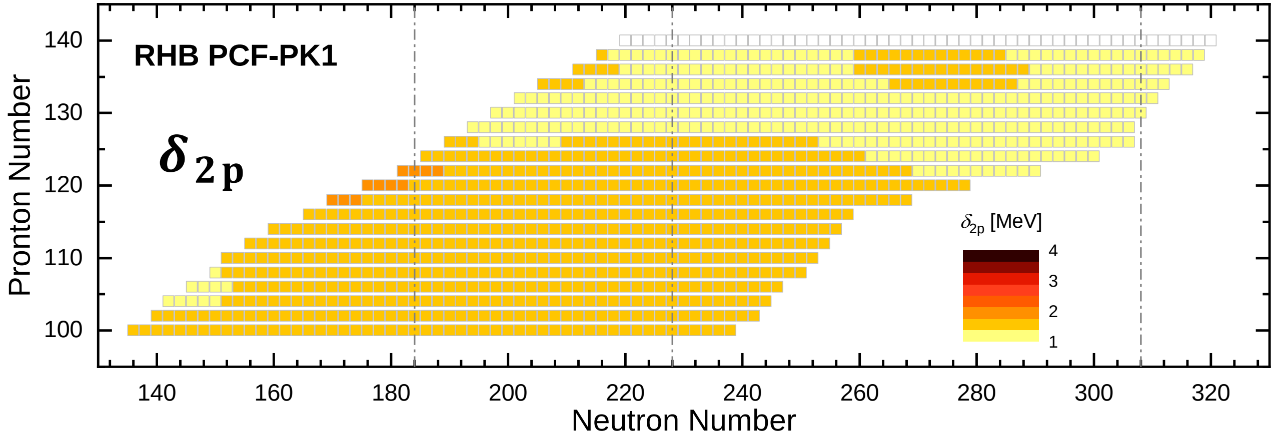

1. PCF-PK1 supports the neutron magic number **184, 228** and **308**. Shell gaps of 228 and 308 are weaker than 184.
2. No obvious proton magic number.

Why Shell Gaps are So Small

- S. p. energy level of $^{292}120$

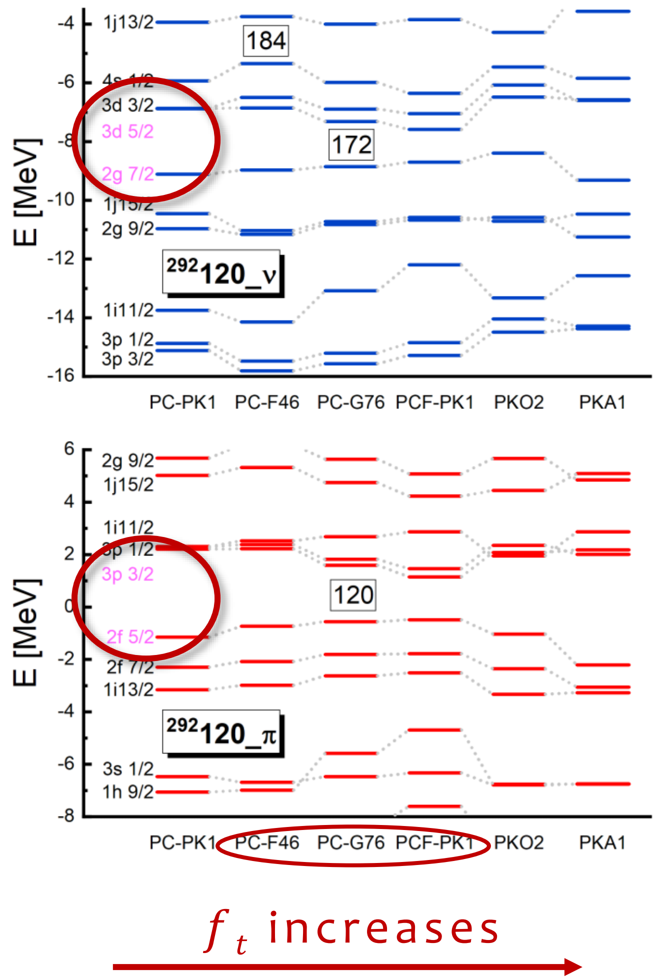

1. $Z = 120$ is regarded as magic number in many functionals.
2. Energy splittings of pseudospin doublets $\Delta E_{\mathrm{PSO}}(\nu 2\tilde{f})$ and $\Delta E_{\mathrm{PSO}}(\pi 2\tilde{d})$ are **small**, compared with other functionals, so the shell gaps of 120 and 172 are weak.
3. ΔE_{PSO} **decreases** with tensor coupling strength f_t and Σ_0 increasing.

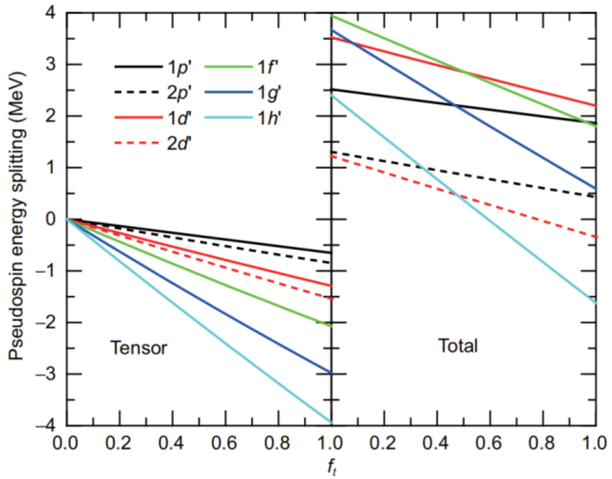

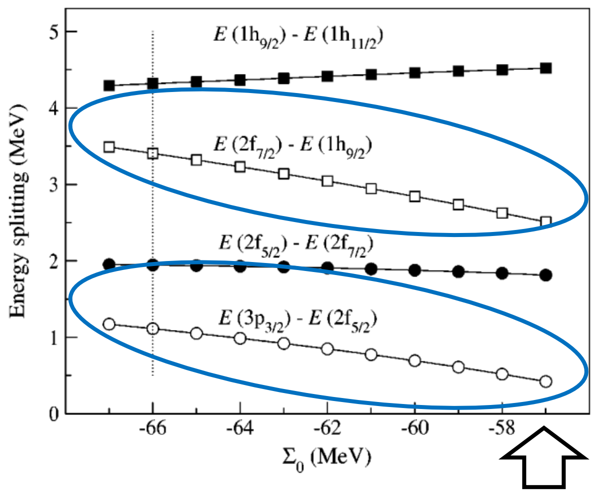

S. W. Chen et al.,2016,Sci.Chin. 59,682011
P. Alberto et al.,2002,PRC 65,034307

S. p. Energy Level of Heavy Nuclei

➢ S. p. energy level of doubly magic nuclei ^{132}Sn and ^{208}Pb

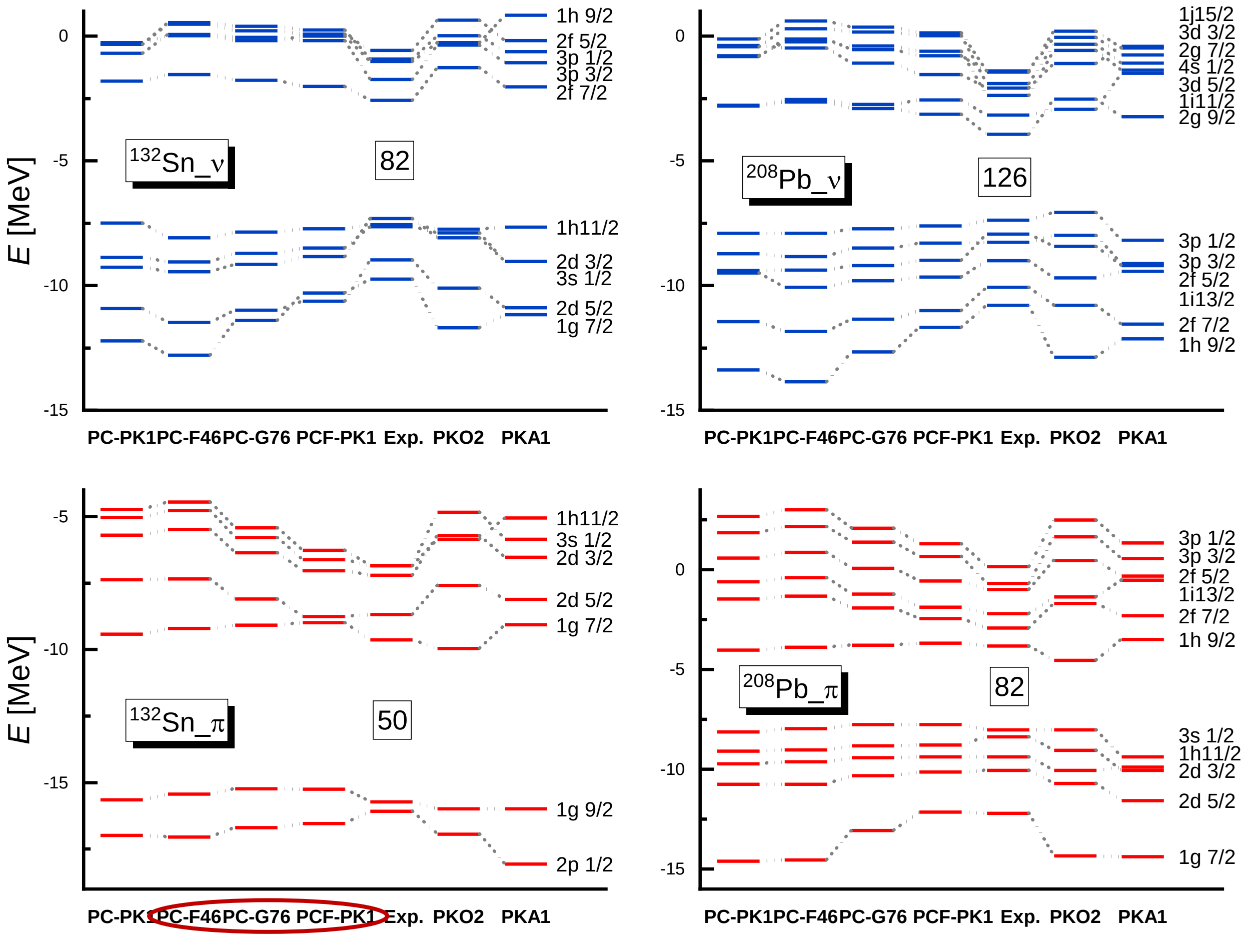

f_t increases

1. S. p. energy level : in good agreement with the experiment value, which indicates the extrapolation ability to the SHN region.

V. Isakov et al.,2002,EPJA 14,29

2. Level density: close to the experiment. Level density increases with tensor coupling strength increasing.

Summary

Summary

- **7210 nuclei are predicted to be bound** with RHB theory using functional PCF-PK1. The rms deviation of mass is **7.170 MeV**, which is comparable to PC-PK1.
- **Spurious shell $Z = 58, 92$ are removed** with PCF-PK1.
- **No obvious proton magic number is predicted in SHN region**.

Perspective

- With improved shell structure, **β-decay half-lives** can be calculated by PCF-PK1, which is also one of the most important inputs of nucleosynthesis.

Thanks !

Appendix--status

Name(Y)	Model	Para.	Shape	Pair	Bound	$^{\#}A$	$\sigma(E_b)$	$^{\#}R$	$\sigma(R_{ch})$	Details
D.Hirata, 1997	RMF	TMA	axial	no	2174(8-120)	-	2.71	-	-	H.O.
G.A.Lalazissis, 1999	RMF+BCS	NL3	axial	const.	1315(10-98)	-	2.6	-	-	H.O.
L.Geng, 2005	RMF+BCS	TMA	axial	δ-force	6969(8-100)	2882 642*	2.118 2.113*	523 -	0.037 -	H.O.
J.Meng, 2013	RMF+BCS	PC-PK1	axial	δ-force	~2000(≥8)	-	1.422	-	-	H.O.
Q.S.Zhang, 2014	RMF+BCS	PC-PK1	axial	δ-force	575(8-108)	575	1.24	-	-	
K.Q.Lu, 2015	RMF+BCS	PC-PK1	triaxial	sep.	575(8-108)	575	1.14	-	-	
A.V.Afanasjev, 2013 S.E.Agbemava, 2014	RHB	NL3*	axial	sep.	2216(≤120)	- 638*	2.97 2.907*	- -	0.0407 -	H.O.
		DD-ME2			2050(≤120)	- 636*	2.42 2.377*	- -	0.0376 -	
		DD-MEδ			2057(≤120)	- 634*	2.31 2.309*	- -	0.0412 -	
		DD-PC1			2040(≤120)	- 636*	2.02 2.019*	- -	0.0402 -	
X.Y.Qu, 2013	RCHB	PC-PK1	spherical	δ-force	402(8-22)	234	2.23	-	-	shooting
X.W.Xia, 2018	RCHB	PC-PK1	spherical	δ-force	9035(8-120)	2284 630*	7.960 8.036*	- -	0.0358 -	shooting
Y.L.Yang, 2020	RHB	PC-PK1	triaxial	sep.	569(8-50)	252	1.59	-	-	H.O.
Y.L.Yang, 2021					-(8-104)	- 628*	1.31 1.335*	- -	- -	
K.Zhang, 2022	DRHBc	PC-PK1	axial	δ-force	2583(8-120)	637	1.518	369	0.032	D.W.S.

spherical

triaxially deform.

Axially deform.

Appendix-- Mass

- Comparison of mass accuracy

Version	RHB PCF-PK1	σ_{rms}/MeV	RCHB PC-PK1	σ_{rms}/MeV	
AME2003	2085	6.938	2111	7.884	G.Audi,2003,NPA 729,337
AME2012	**2258**	**7.026**	**2285**	**7.958**	M.Wang,2012,CPC 36,1603
AME2016	2301	6.996	2331	7.917	M.Wang,2017,CPC 41,030003
AME2020	**2351**	**7.170**	**2382**	**8.103**	M.Wang,2021,CPC 45,030003

σ (magic nuclei)=2.034 MeV, which is also lower than 2.157 MeV in PC-PK1.

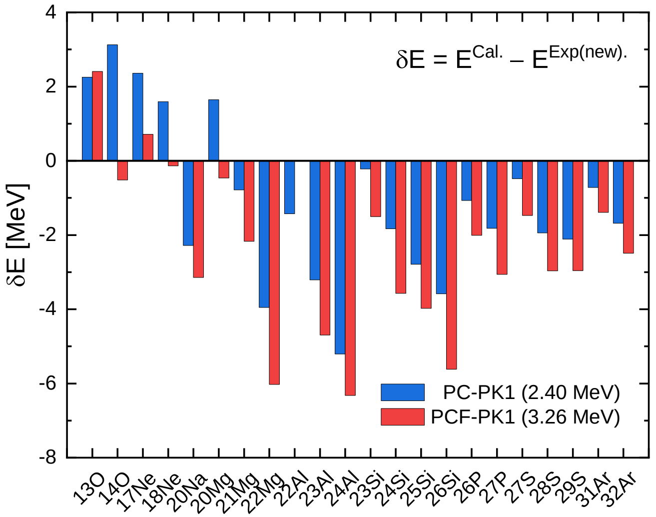

For newer data, PCF-PK1 is higher than PC-PK1 0.8 MeV.

Data from IMP report

Appendix-- Separation Energy

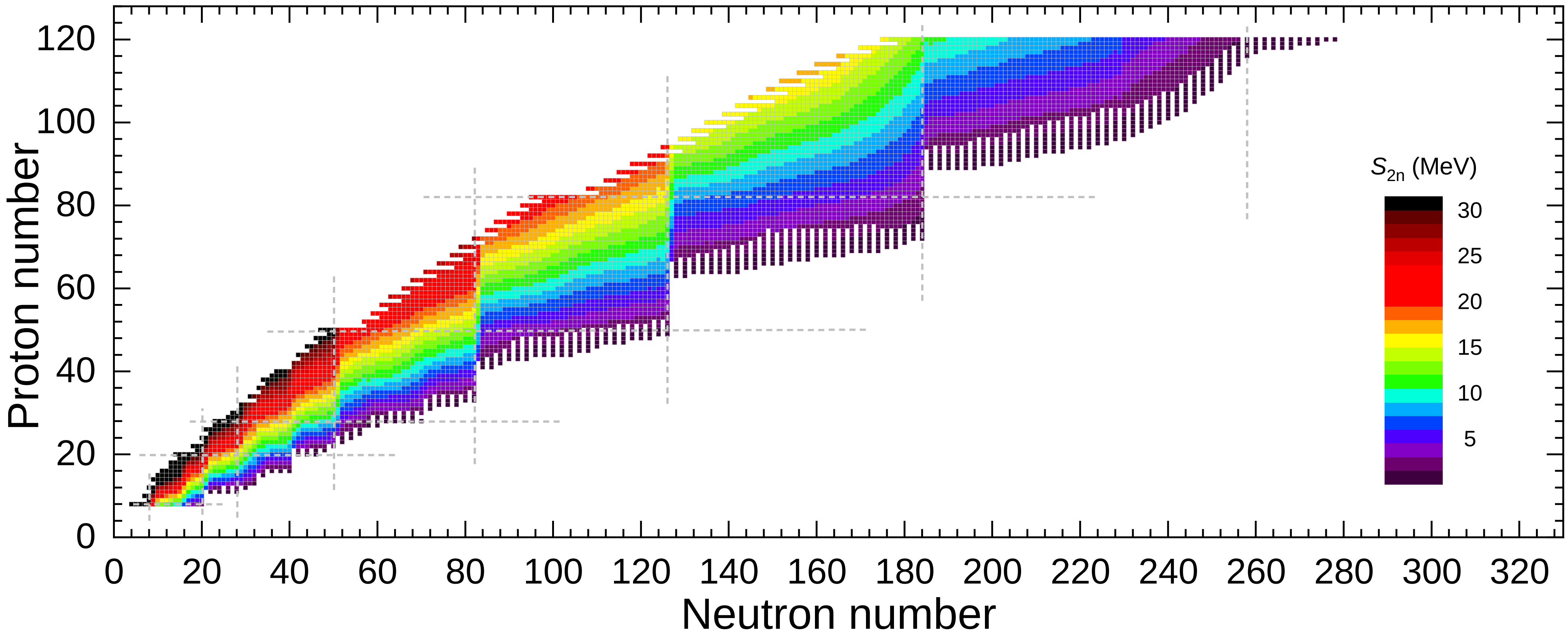

- 2149个核$S_{2n} \leq 5$ MeV，645个核$S_{2n} \leq 2$ MeV。
- $S_{2n} \geq 20$ MeV的有606个，大部分位于$Z \leq 80, N \leq 82$区域，小部分(36个)位于$82 \leq Z \leq 94$之间，≥25MeV的有253个，大部分都处于$Z < 50$，小部分(21个)处于$58 \leq Z \leq 70$之间，≥30MeV的有103个核且都处于$Z < 50$区域，≥40MeV的有7个核，分别是^{12}O，^{13}O，^{17}Ne，^{20}Mg，^{23}Si，^{34}Ca，^{35}Ca。

Appendix-- Separation Energy

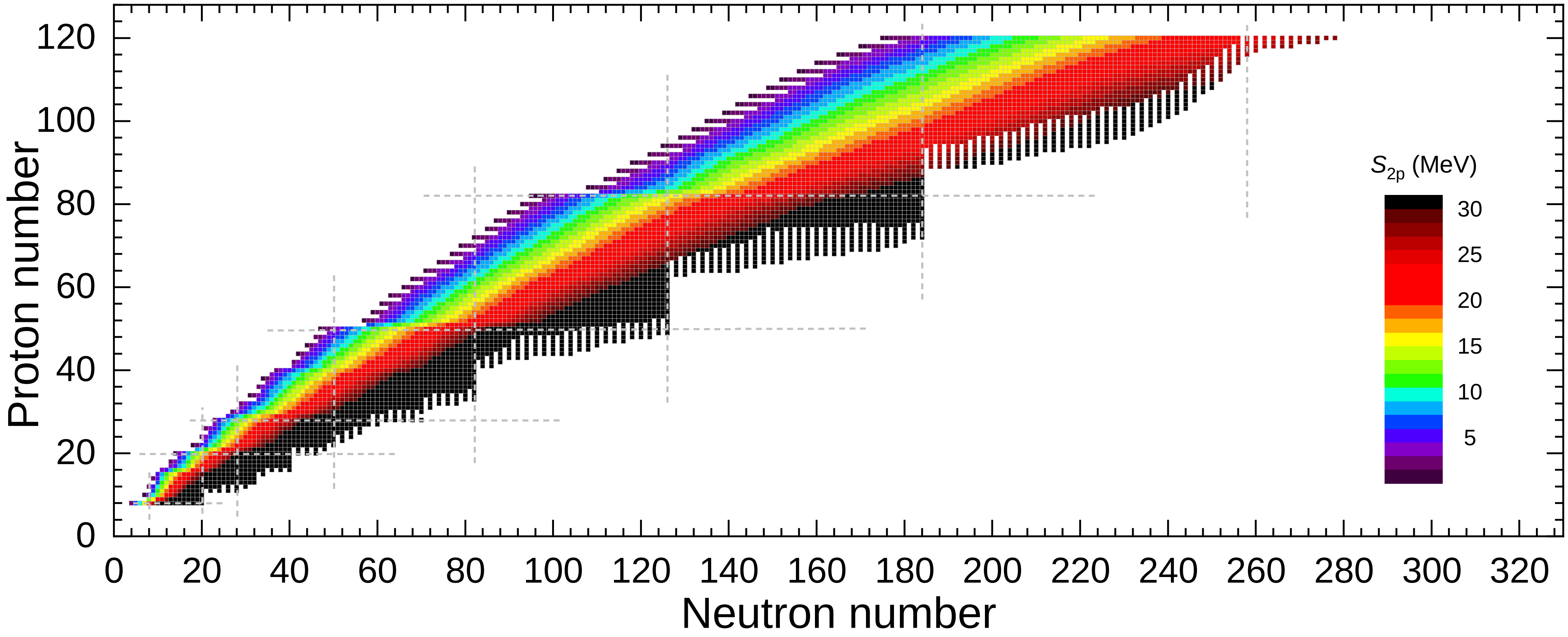

- 485个核S_{2p}≤5MeV，101个核S_{2p}≤2MeV。
- S_{2p}≥20MeV的有3807个核，≥25MeV的有2665个核，≥30MeV的有1636个核，≥40MeV的有440个，且大部分位于Z≤60,N≤126区域，有38个核S_{2p} > 50MeV，基本都位于Z≤20区域。

Appendix-- Separation Energy

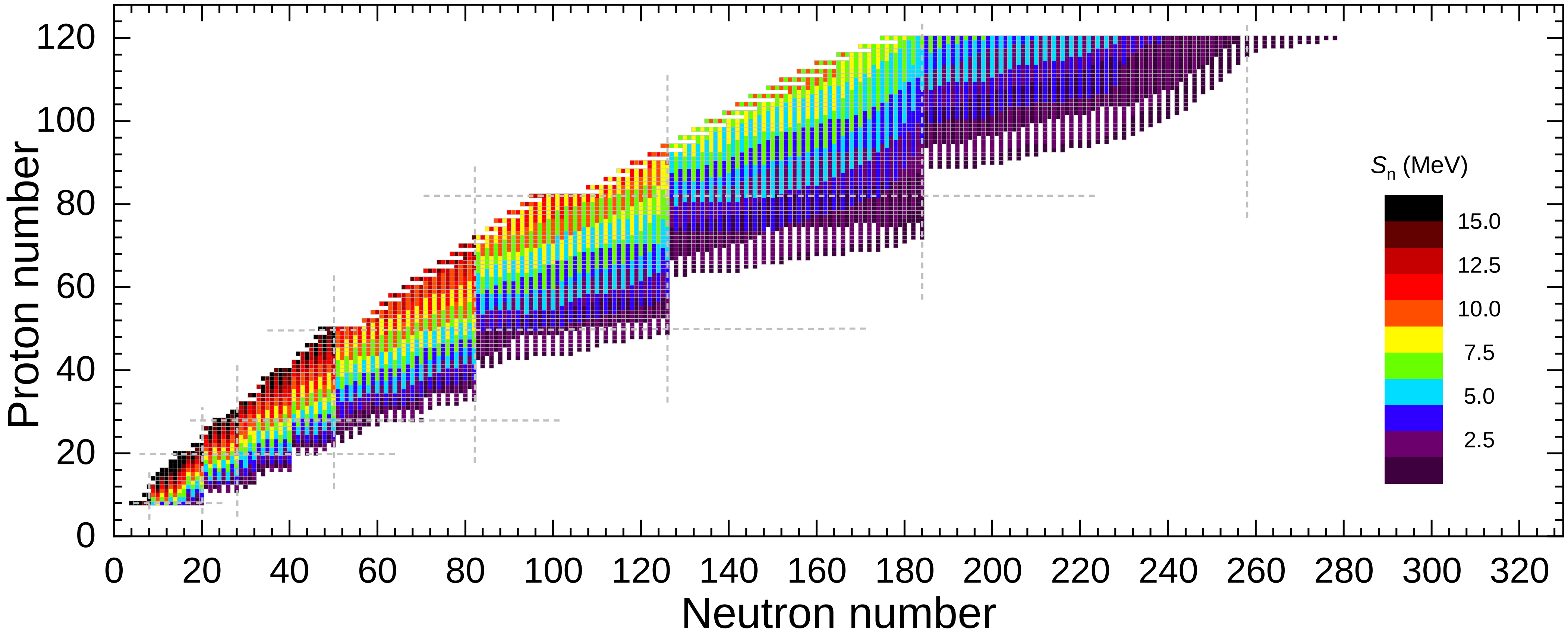

- $S_n \leq 5$MeV的核有4221个，1679个核的$S_n \leq 2$MeV，295个核的$S_n \leq 0.5$MeV，且中子数基本是奇数，63个核的$S_n \leq 0.1$MeV。
- $S_n \geq 10$MeV的有646个核，基本位于$N<126$区域，93个核的$S_n \geq 15$MeV，都位于$N \leq 50$区域，^{12}O，^{14}O，^{20}Mg，^{25}P，^{32}Ar，^{34}Ca这几个核的$S_n \geq 20$MeV。
- 同S_{2n}，可以看出跨过幻数后S_n会有较大的变化。而且S_n有奇偶效应，靠近滴线时偶中子核的S_n大于奇中子核。

Appendix-- Separation Energy

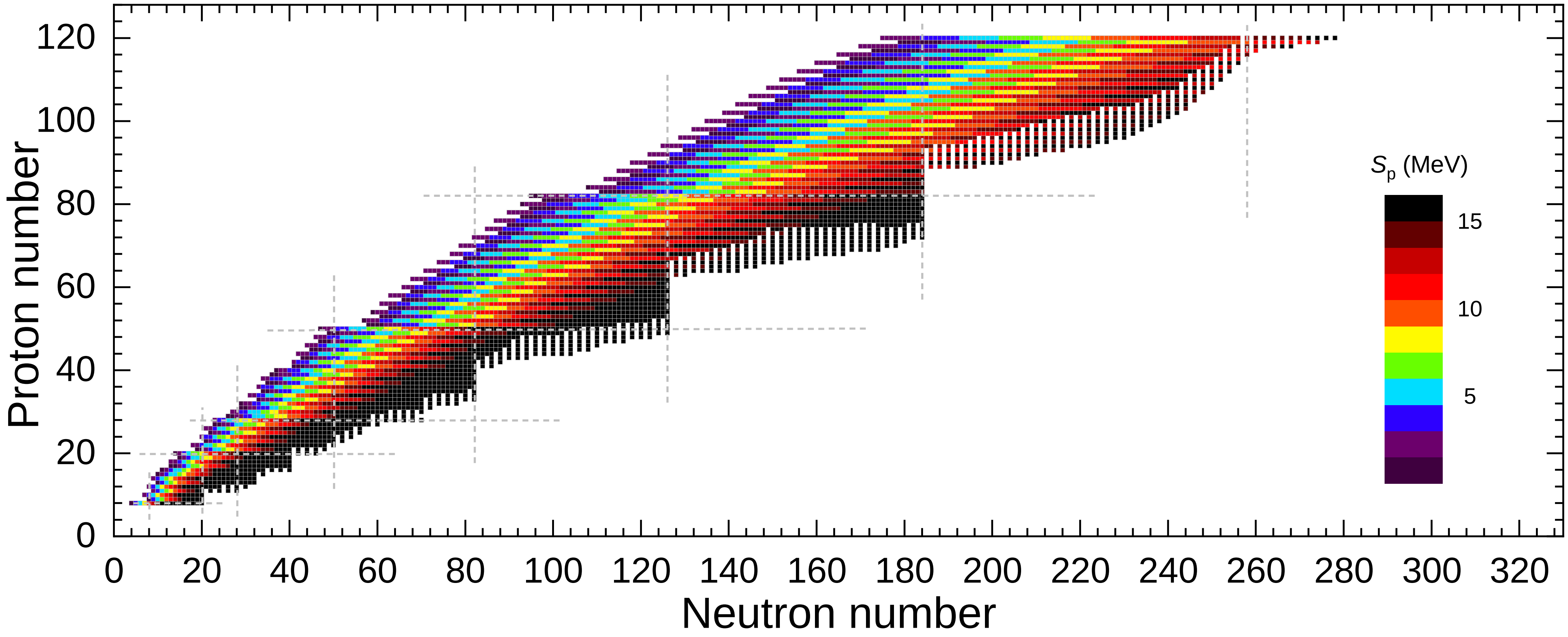

- 1501个核$S_p \leq 5$MeV，417个核$S_p \leq 2$MeV，80个核$S_p \leq 0.5$MeV，15个核$S_p \leq 0.1$MeV。
- $S_p \geq 10$MeV的核有3668个，≥ 15MeV的有1601个，≥ 20MeV的有424个，处于$N<184$，$Z<82$区域内，≥ 25MeV的有43个，都处于$N<126$，$Z \leq 50$区域内。
- 同S_{2p}，$Z=20$，28，50，82后S_p有较大变化，并且同中子素链上偶质子核S_p大于奇质子核。

Appendix-- Separation Energy and Gap with Magicity

- 幻数核的分离能和壳隙与实验的差别

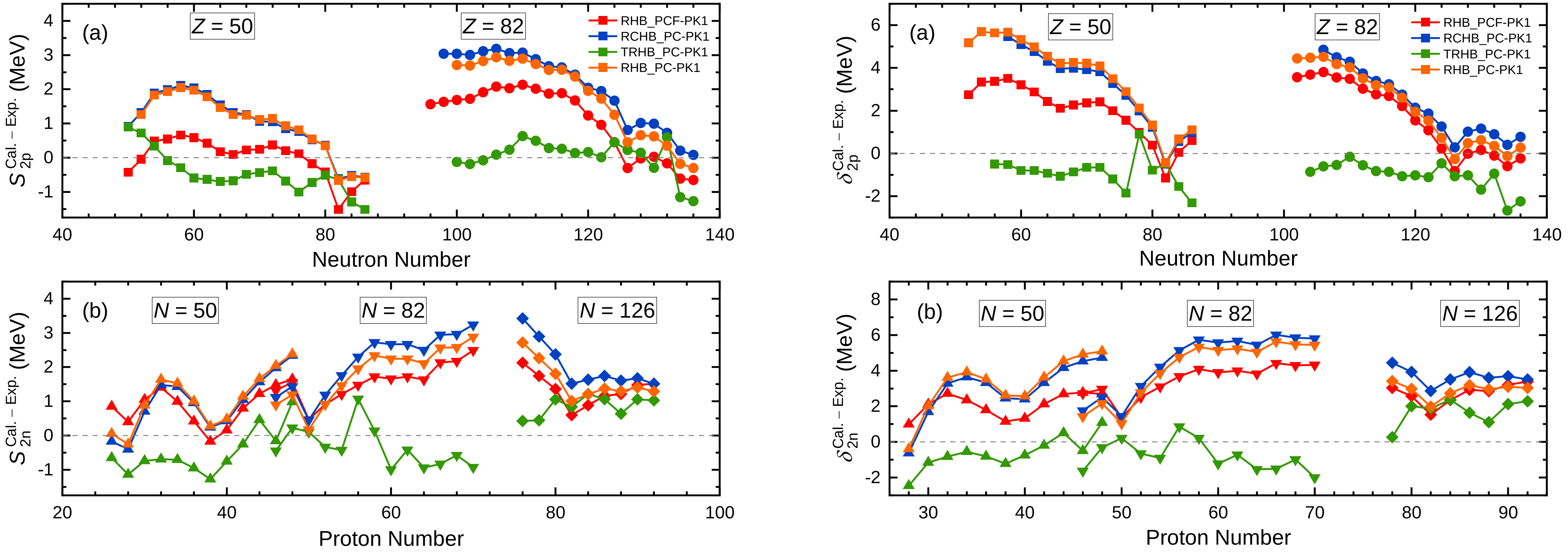

1. PCF-PK1的分离能和壳隙与实验的偏差较小，与PC-PK1的描述接近，特别在双幻核附近二者没有表现出较大差别。从理论与实验偏差的变化趋势说明在超重核区实验会倾向于更小的壳隙。
2. 当考虑形变以及动力学修正能后，理论与实验的偏差得到修正。

Appendix-- Charge Radii

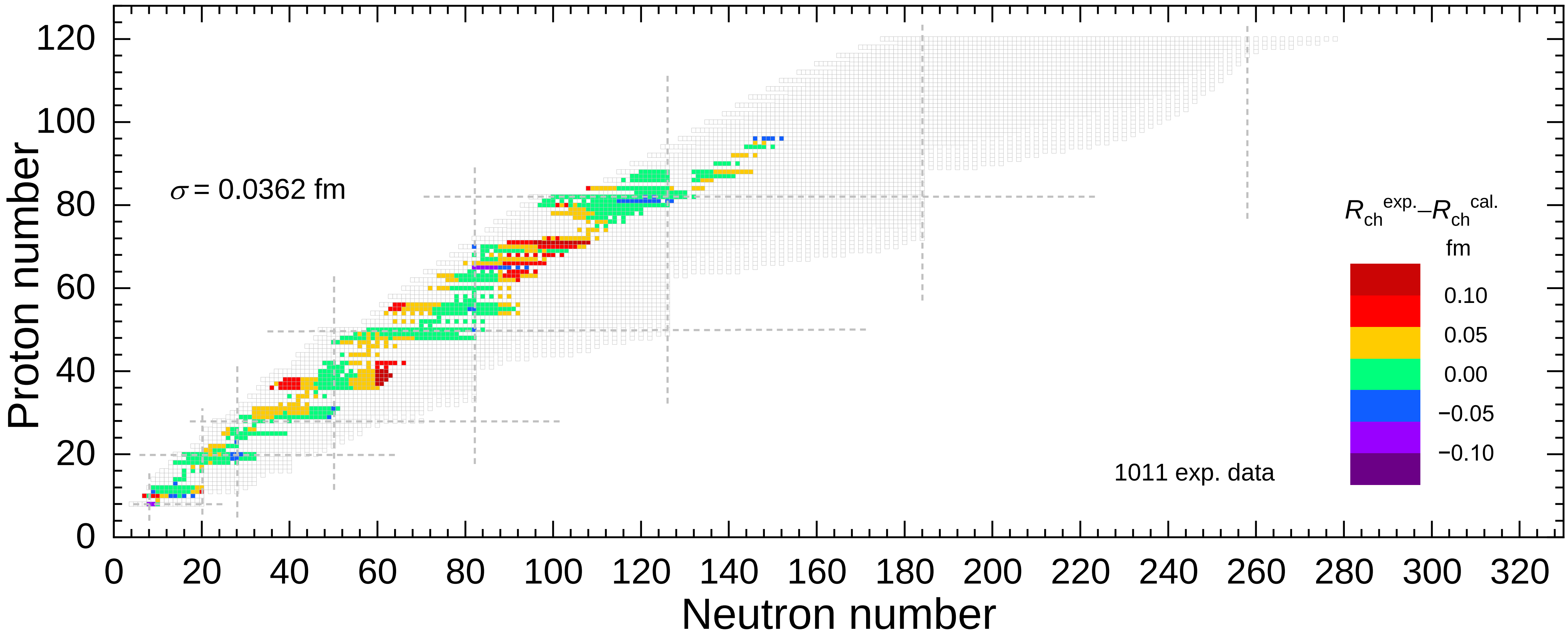

- 与1011个实验数据的方均根偏差为0.0362fm，略高于Xia对电荷半径的$\sigma = 0.0358$ fm。
- 幻数附近的精度普遍较高，两个闭壳之间的绝对误差普遍较大。

Appendix-- α-Decay Energy

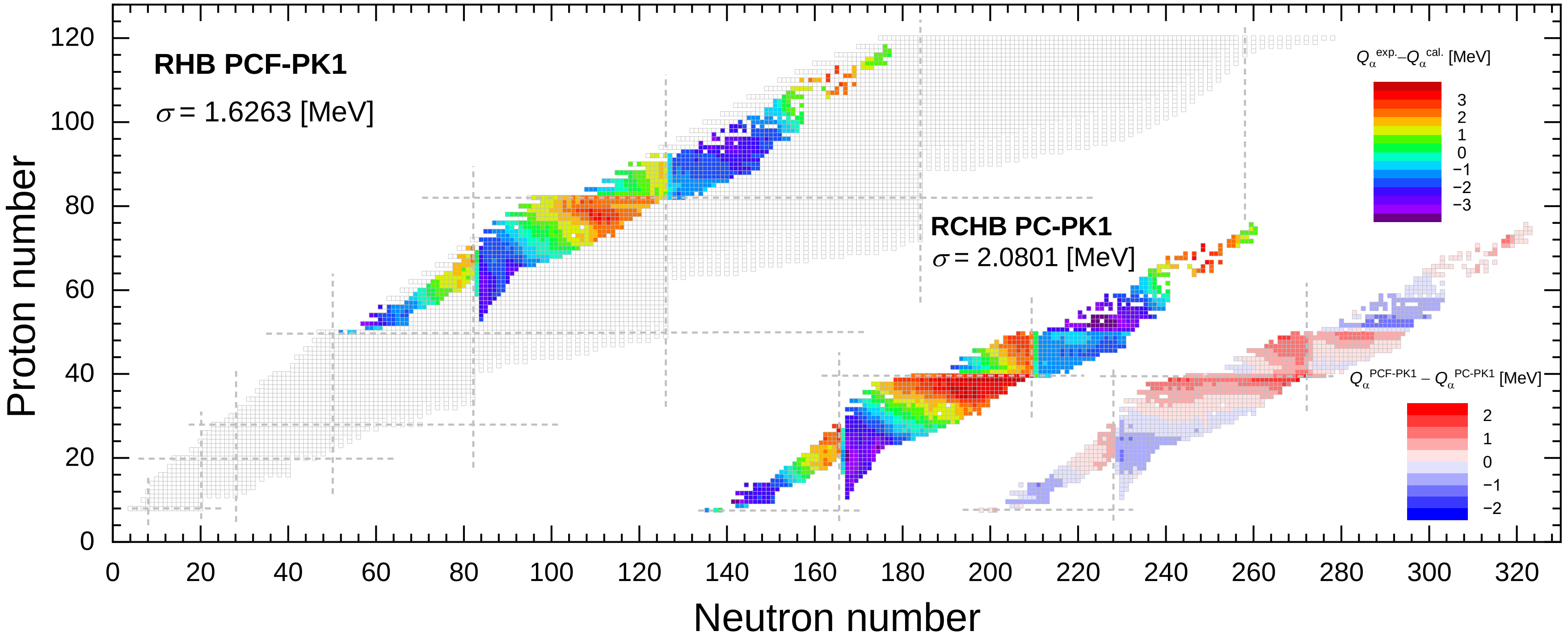

1. 在幻数附近，RHB与RCHB的Q_α差别明显，形变区域差别不大，暗示PCF-PK1对壳结构的描述更合理。
2. 在超重核区，即使是形变区域也有改善。而且$Z=92$分界线以上PCF-PK1的描述更接近实验值一些，说明消除赝壳有助于改善Q_α的描述。

Spurious Shell Removal

Proton	$^{142}_{60}$Nd		$^{144}_{62}$Sm		$^{214}_{88}$Ra		$^{216}_{90}$Th		$^{220}_{94}$Pu		$^{222}_{96}$Cm	
PCF-PK1	5.25	0.99	5.17	1.07	4.01	1.59	3.97	1.68	3.91	1.77	3.90	1.77
DD-LZ1	6.63	2.07	6.56	1.96	5.26	2.00	5.13	2.13	4.94	2.25	4.89	2.24
PC-PK1	5.81	2.57	5.78	2.55	4.16	2.86	4.12	2.93	4.05	3.00	4.01	3.01
DD-PC1	5.80	2.69	5.76	2.72	4.01	3.18	4.01	3.22	3.99	3.29	3.96	3.31
DD-ME2	5.97	2.96	5.92	2.89	4.16	3.10	4.12	3.20	4.06	3.28	4.04	3.28

E_B (MeV)	^{142}Nd	^{144}Sm	^{214}Ra	^{216}Th	^{220}Pu	^{222}Cm
PCF-PK1	1185.77	1196.00	1660.36	1664.76	1668.78	1668.48
DD-LZ1	1184.39	1194.76	1659.04	1663.63	1667.87	1667.56
PC-PK1	1186.48	1196.44	1661.97	1666.97	1671.14	1670.48
DD-PC1	1190.17	1199.76	1664.95	1670.08	1673.94	1672.85
DD-ME2	1187.16	1196.90	1663.71	1669.19	1673.73	1672.94
Exp.	**1185.13**	**1195.63**	**1658.29**	**1662.55**	**-**	**-**

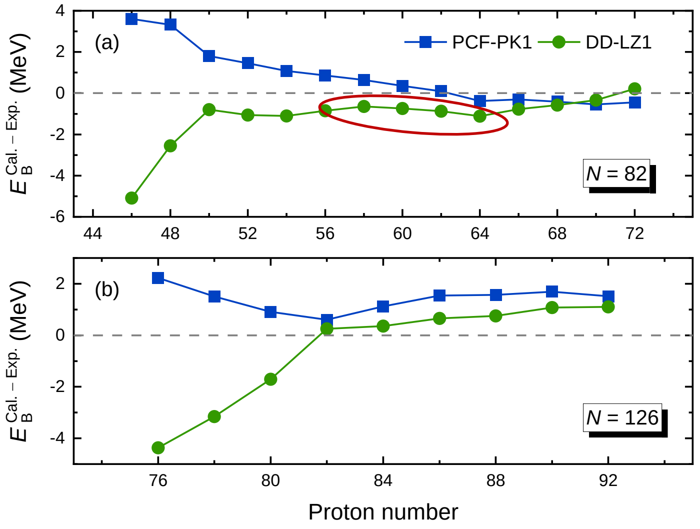

- PCF-PK1对58以及92壳隙描述相对较小，因此关键原子核的质量更接近实验值。同样地，DD-LZ1($M_S^* = 0.56$)描述50和82的壳隙明显较大，这可能与质量的低估有关。问题：^{214}Ra与^{216}Th如何解释。

Appendix-- Shell Gap in light region

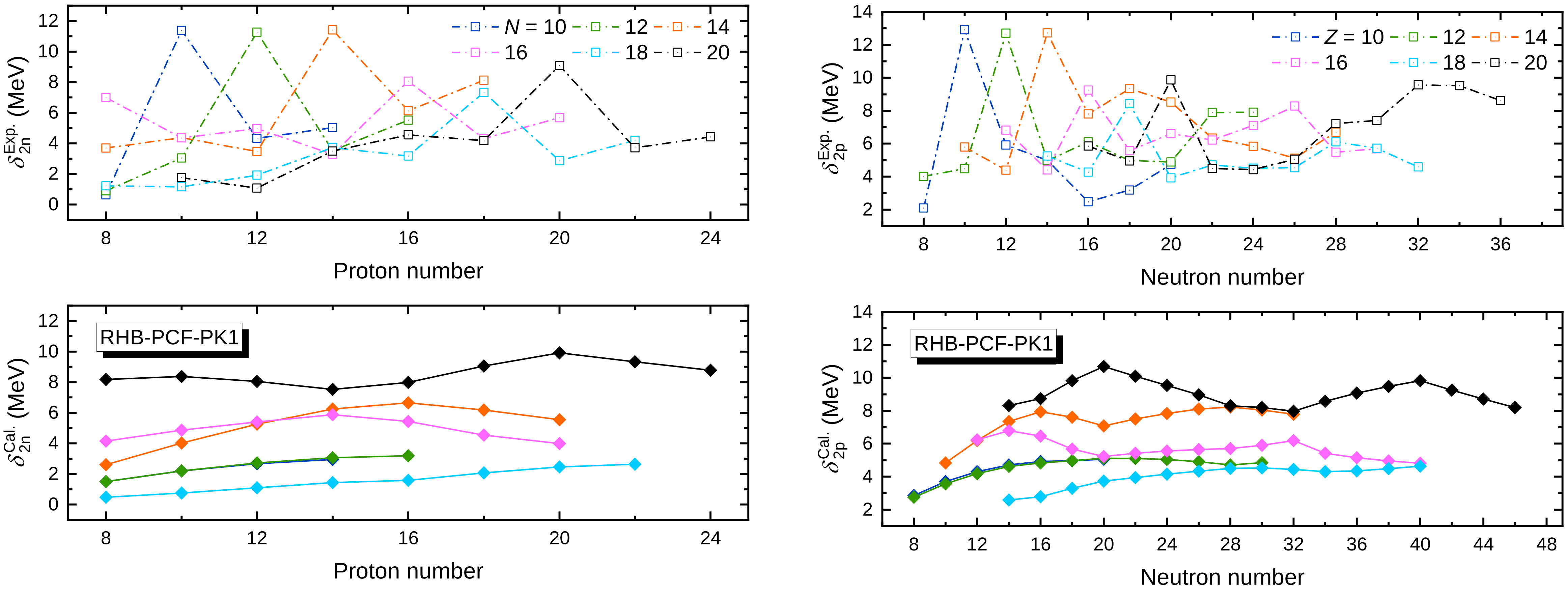

- 当$N = Z$时，实验壳隙出现极大值，也许和对称能相关，无中子剩余的体系能量更低。
- PCF-PK1在$N = 14$时，$Z = 16$出现极大，而$N = 16$时，$Z = 14$出现极大；同双质子壳隙。

Appendix-- Shell Gap in light region

- RCHB对应的计算结果

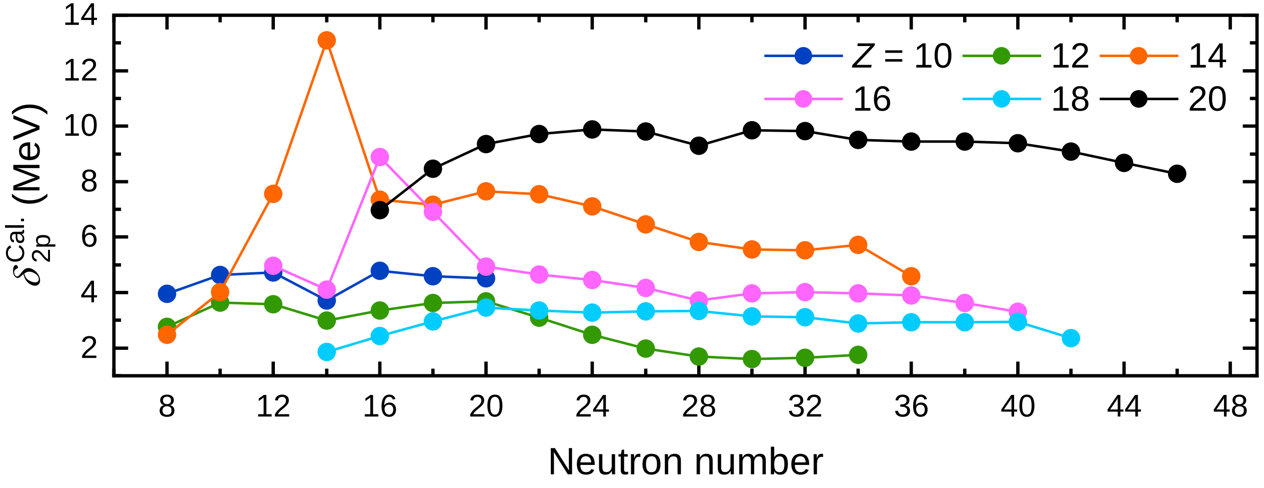

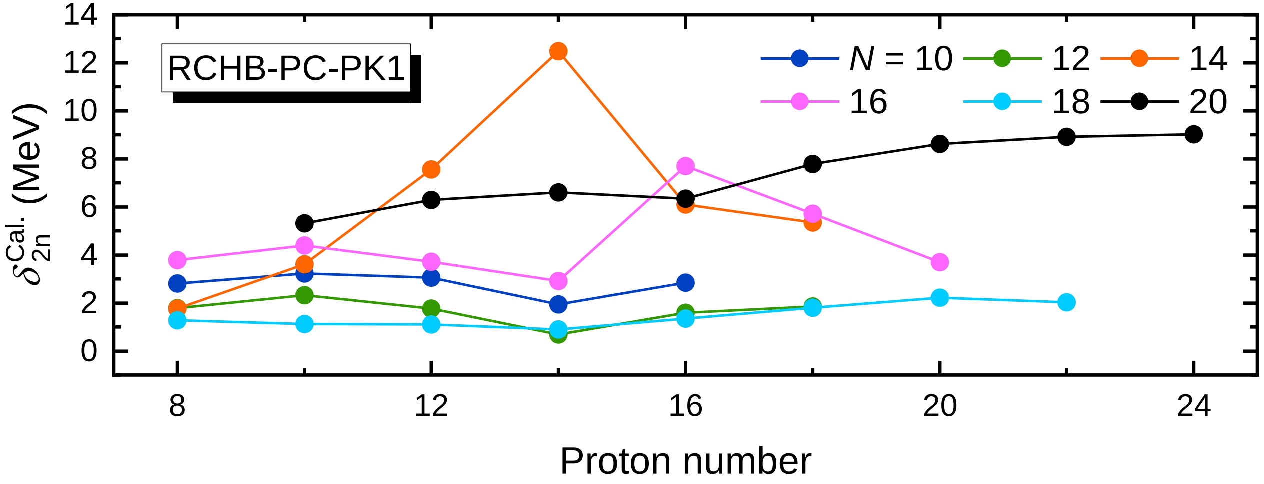

- RCHB在 $N, Z = 14, 16$ 处重现实验的现象。

Appendix-- Neutron Magicity in ^{52,54}Ca

- Ca同位素链双中子分离能(红)，对能(蓝)，以及Δ_{2n}与δ_e。

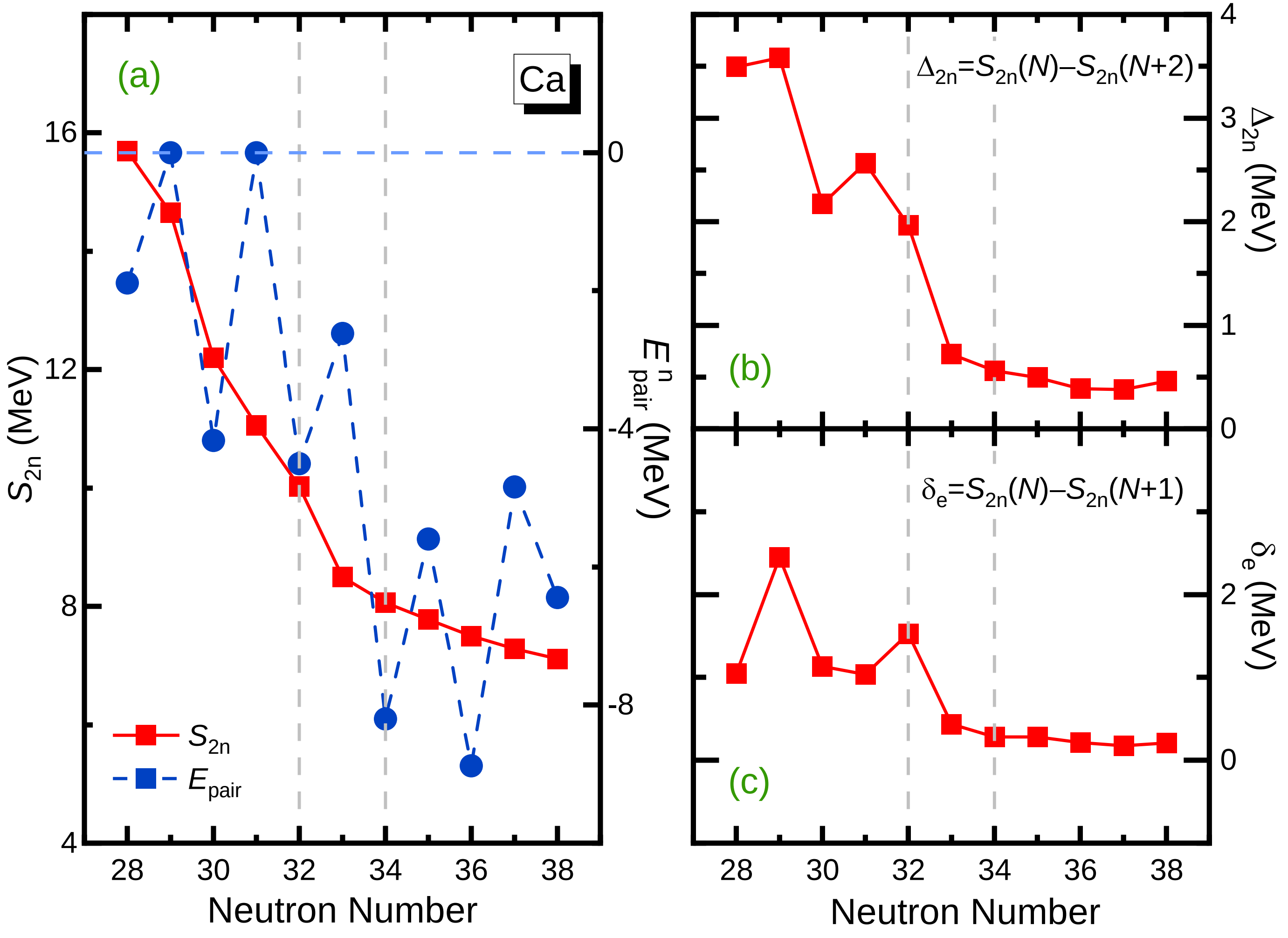

- (a)^{52}Ca的双中子分离能略高于^{53,54}Ca，但S_{2n}(^{54}Ca)并未明显高出附近核。
- (b)Δ_{2n}(^{52,54}Ca)并未明显高于其他核，而^{50,51}Ca较高。
- (c)δ_e(^{52}Ca)高于附近核，但^{54}Ca明显没有类似现象说明N=32的中子幻数不明显，而且并未重现中子幻数34。

Appendix-- Double-Magic nuclide ^{270}Hs

- 不同链Q_α随中子数的变化

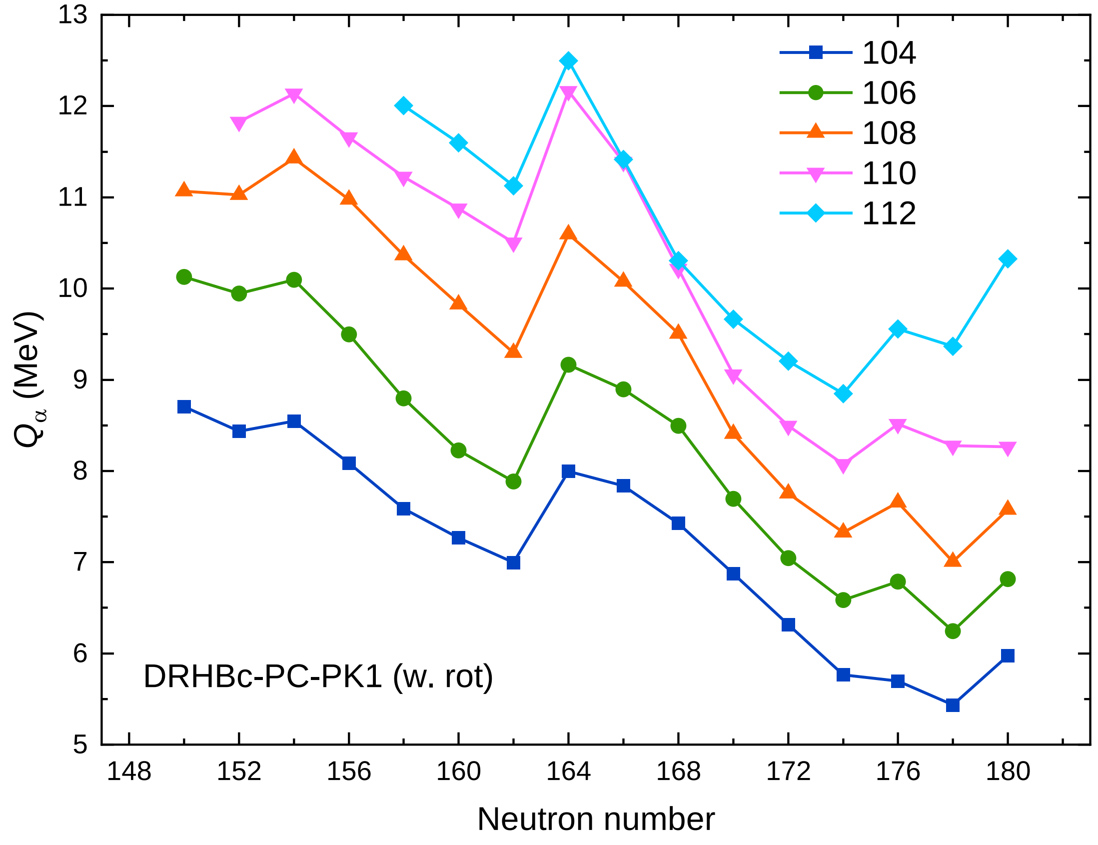

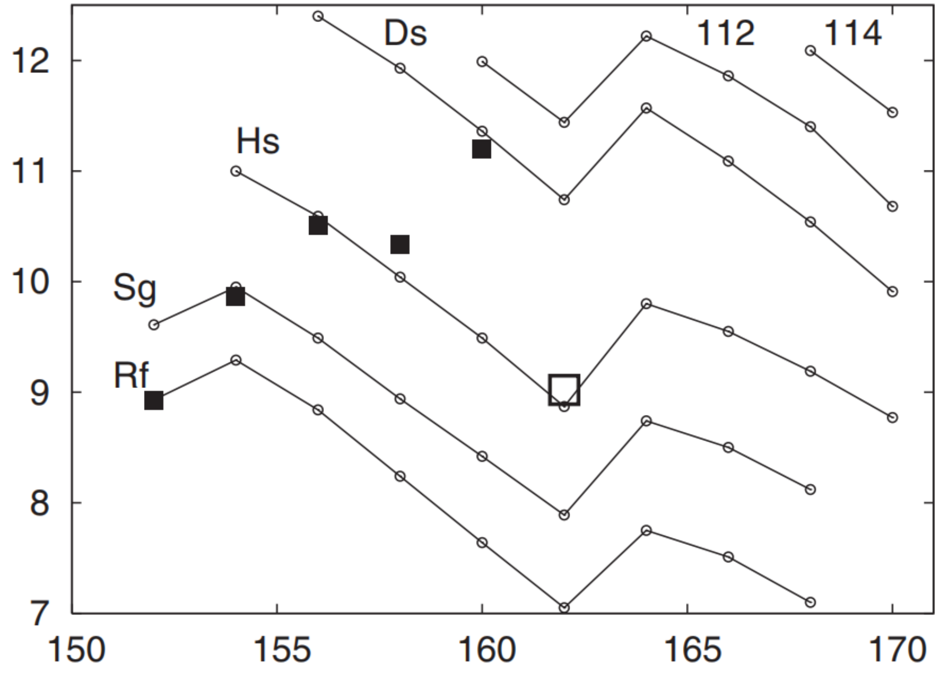

J.Dvorak,2006,PRL,97,242501

Appendix-- Superheavy Double Magic Nucleus ^{270}Hs

- Q_α with respect to Hs isotopes

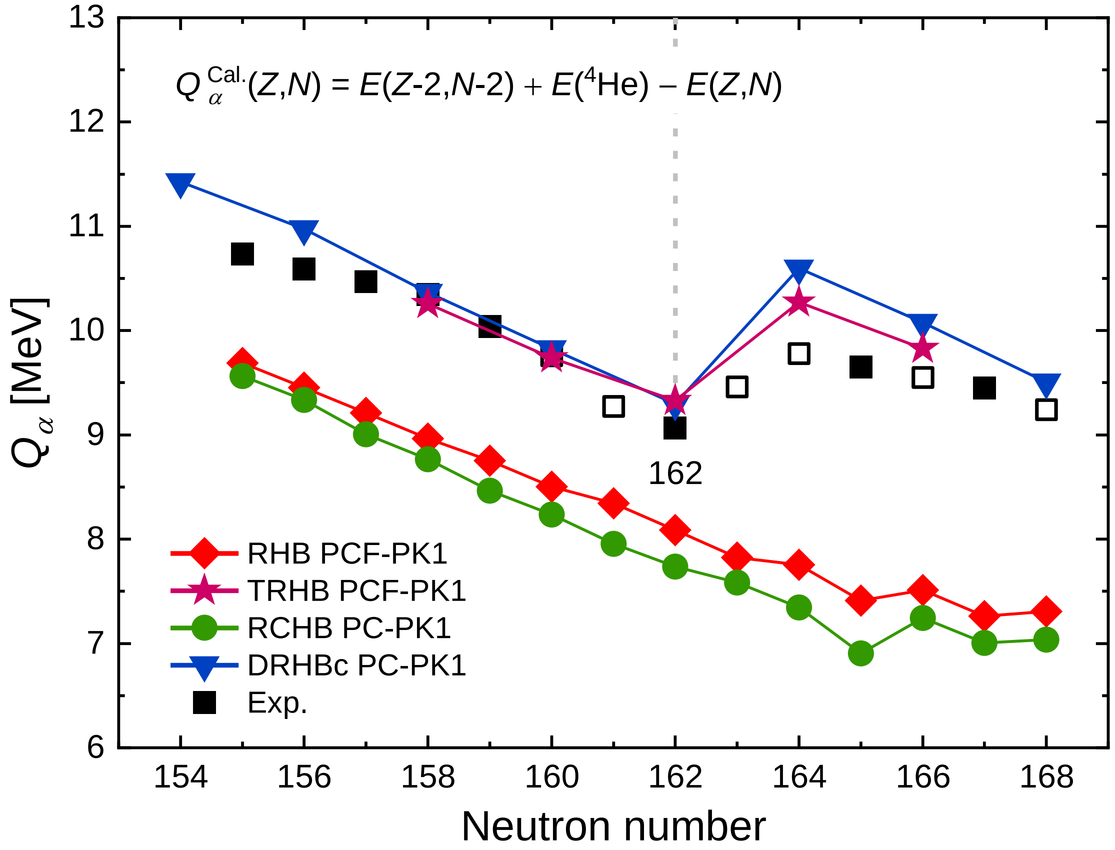

J.Dvorak,2006,PRL 97,242501

1. In spherical case, PCF-PK1 do not reproduce $N = 162$(deformed magic number?).
2. PCF-PK1(TRHB) supports the deformed magic number 162, so as PC-PK1(DRHBc). And the peak magnitude of PCF-PK1 is weaker.

Appendix-- Level Density

- 双幻核^{208}Pb的单粒子能级密度

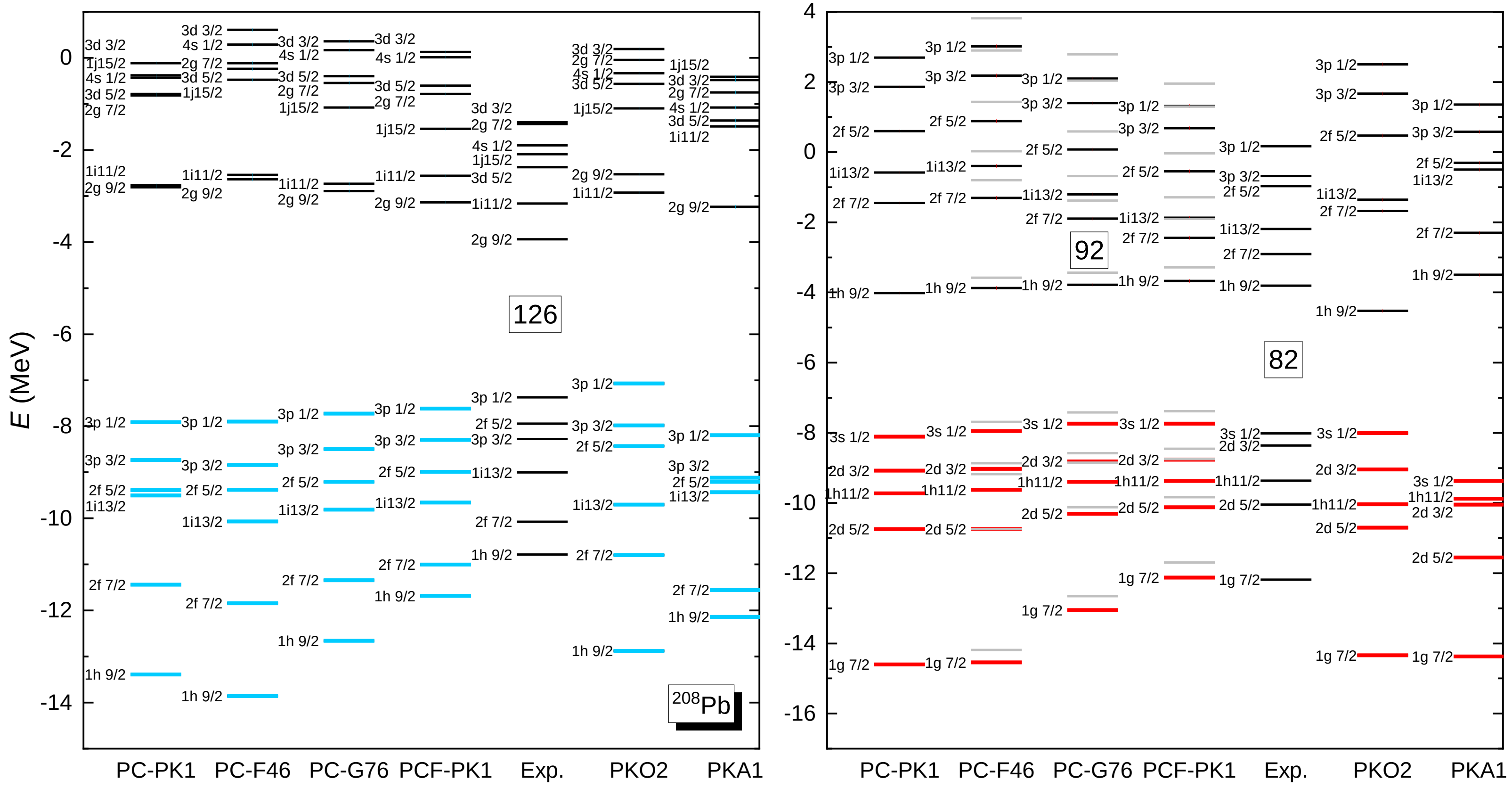

1. PCF-PK1的能级密度最大，且单粒子能量的描述更接近实验值。PKA1的描述与之接近，但PKA1费米面以下的质子能级与实验值偏离较大。
2. ^{210}Po(灰色)未表现出更小的82的壳隙。

Appendix-- Level Density

- $^{304}120$的能级密度随着张量耦合强度的变化

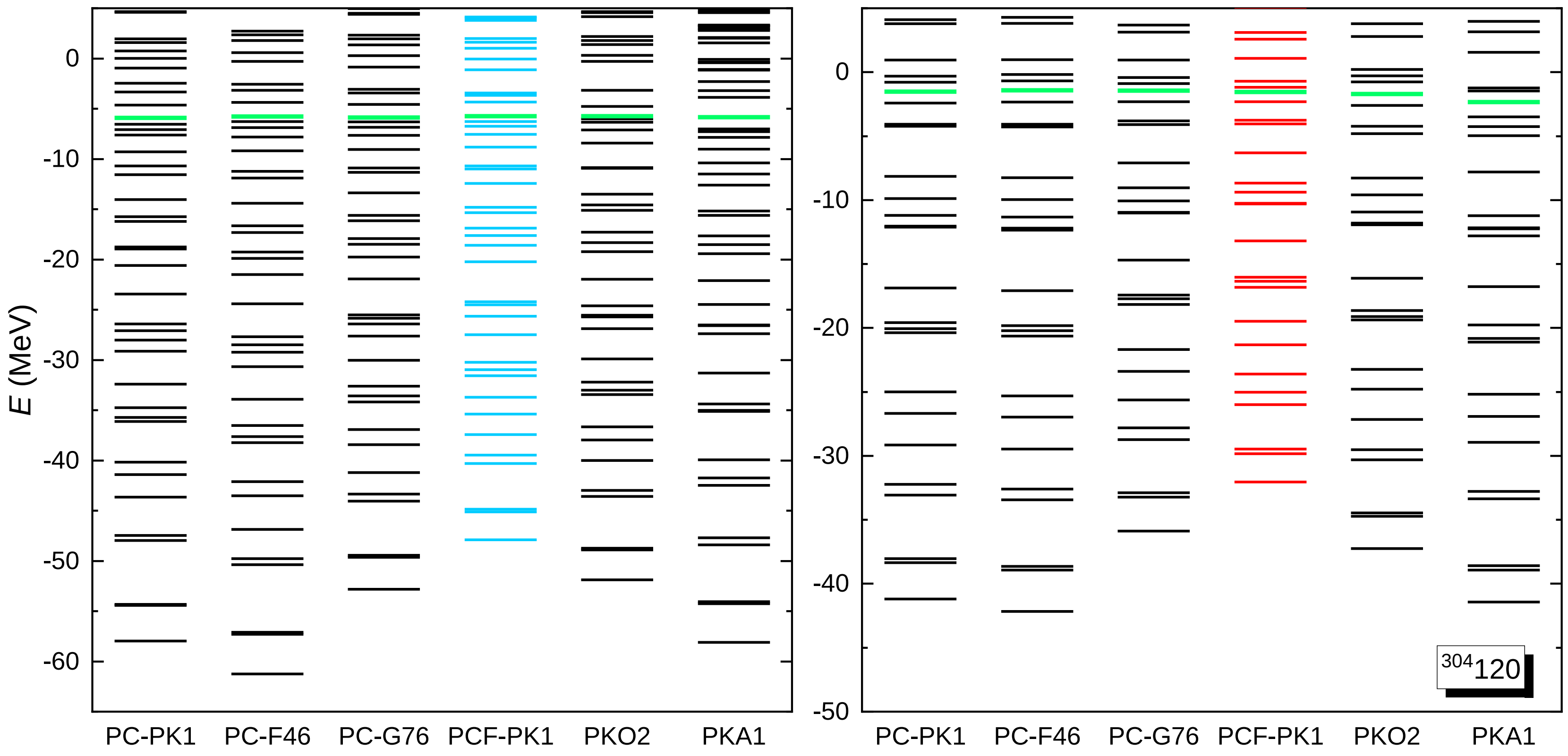

Para.	M_D^*	M_L^*
PC-PK1	0.59	0.65
PC-F46	0.60	
PC-G76	0.70	
PCF-PK1	0.80	0.85
PKO2	0.60	0.74
PKA1	0.54	

总的来说，PCF-PK1对$^{304}120$的单粒子能级的描述明显区别于其他有效相互作用，表现为能级密度较高，壳效应减弱。由于引入张量耦合，PCF-PK1较大的Dirac有效质量会减弱ΔE_{SO}，而较大的Landau有效质量会增大能级密度，最终PCF-PK1的超重核区质子幻数结构不明显。

Acknowledgement

- Prof. Yifei Niu
- Dr. Qiang Zhao, Prof. Pengwei Zhao
- Yilong Yang
- All members of the group